

## Electrically induced patterns in nematics and how to avoid them

N. Éber, P. Salamon & Á. Buka

To cite this article: N. Éber, P. Salamon & Á. Buka (2016) Electrically induced patterns in nematics and how to avoid them, *Liquid Crystals Reviews*, 4:2, 101-134, DOI: [10.1080/21680396.2016.1244020](https://doi.org/10.1080/21680396.2016.1244020)

To link to this article: <http://dx.doi.org/10.1080/21680396.2016.1244020>



Published online: 31 Oct 2016.



Submit your article to this journal [↗](#)



Article views: 142



View related articles [↗](#)



View Crossmark data [↗](#)

REVIEW

## Electrically induced patterns in nematics and how to avoid them

N. Éber, P. Salamon and Á. Buka

Institute for Solid State Physics and Optics, Wigner Research Centre for Physics, Hungarian Academy of Sciences, Budapest, Hungary

### ABSTRACT

Electric field-induced patterns in liquid crystals have been observed and studied for about 50 years. During this time, a great variety of structures, detected under different conditions, have been described; theoretical descriptions were also developed parallel with the experiments and a huge number of papers have been published. The non-vanishing interest in the topic is due to several factors. First, most experimentalists working with new (or even well-known) liquid crystals apply sooner or later an electric field for different purposes and, as a response, often (maybe undesirably or unexpectedly) have to face with emergence of patterns. Second, understanding the complexity of the formation mechanism of regular patterns in a viscous, anisotropic fluid is an extremely challenging theoretical task. Third, specialists in display fabrication or in other applications are also interested in the results; either to make use of them or in order to avoid field-induced patterns. In this review, we attempt to provide a systematic overview of the large amount of published results, focusing on recent achievements, about the three main types of electric field-induced patterns: transient patterns during the Fredericksz transition, flexoelectric domains and electroconvection. As a result of different instability mechanisms, a variety of pattern morphologies may arise. We address the physical background of the mechanisms, specify the conditions under which they may become effective, discuss the characteristics of the patterns, and summarize the possibilities of morphological transitions induced by frequency, voltage or temperature variations. Special emphasis is given to certain topics, which recently have gained enhanced interest from experimental as well as theoretical point of view, like driving with ultra-low frequencies or non-sinusoidal (superposed) waveforms, and the dynamics of defects and embedded colloidal particles. Assisting newcomers to the field, we also mention some, yet unresolved, problems, which may need further experimental and/or theoretical studies.

### ARTICLE HISTORY

Received 29 July 2016  
Accepted 29 September 2016

### KEYWORDS

Nematic liquid crystals;  
pattern formation;  
electroconvection;  
flexoelectricity

## 1. Introduction

The motivation to review and summarize this topic is obvious; in the large number of liquid crystal (LC) experiments aiming at understanding basic phenomena (fundamental research) as well as in the majority of the LC applications the sample is subjected to electric field. It can lead to a great variety of phenomena depending on many parameters. It is essential for both research and technology to know and predict the field-induced effects; specifically, whether the applied voltage induces a homogeneous state or a structured one. Some researchers intend to study patterns, thus they will prefer them; others, on the contrary, want to avoid patterns regarding them as distractions. Whatever is the actual aim, the onset condition of a pattern is the essential information for a given system. One has to calculate and/or measure the stability limit, which defines the border between the pattern forming and the initial state. Knowing that, one can decide,

whether to remain on the stable or on the unstable side of this limit.

Nematic liquid crystals are vital commodities of our age of information technology; the various devices based on them boosted new branches of the industry and highly contributed to the development of the economy. The great scientific and commercial success of nematics is due to their unique virtues. They possess a long-range orientational order characterized by their cylindrical symmetry axis, the director  $\mathbf{n}$ , which leads to anisotropic physical properties and thus allows easy alignment via interactions with bounding surfaces and with external (electric or magnetic) fields [1,2]. While typical applications (liquid crystal displays) are relied on the homogeneity of the initial and the realigned state, liquid crystals, being in principle nonlinear systems, are easily subjected to pattern forming instabilities [3]. In the present review, we will focus on patterns induced by an electric field.

In a vast majority of scientific studies as well as in applications, nematic liquid crystals are sandwiched as 3–50  $\mu\text{m}$  thick layers between two substrates (either glass or flexible polymer plates), which are coated with transparent electrodes (typical area: 1–400  $\text{mm}^2$ ); thus, the samples have a large ( $> 100$ ) aspect ratio. In the investigations presented below, a similar geometry is utilized. Applying an electric field along  $x$ ,  $y$  or  $z$  to a nematic liquid crystal, homogeneously aligned in the  $x$ – $y$  plane (basic state), might lead to three types of responses:

- no change in the structure (i.e., the basic state is stable);
- transition to a state distorted only along  $z$ , but still homogeneous in the  $x$ – $y$  plane (e.g., a uniform Fredericksz transition [1,2]; Figure 1 depicts the possible geometries);
- onset of a broad variety of three-dimensional patterns [3] (spatially periodic or localized director distortions, which brake the homogeneity in the  $x$ – $y$  plane).

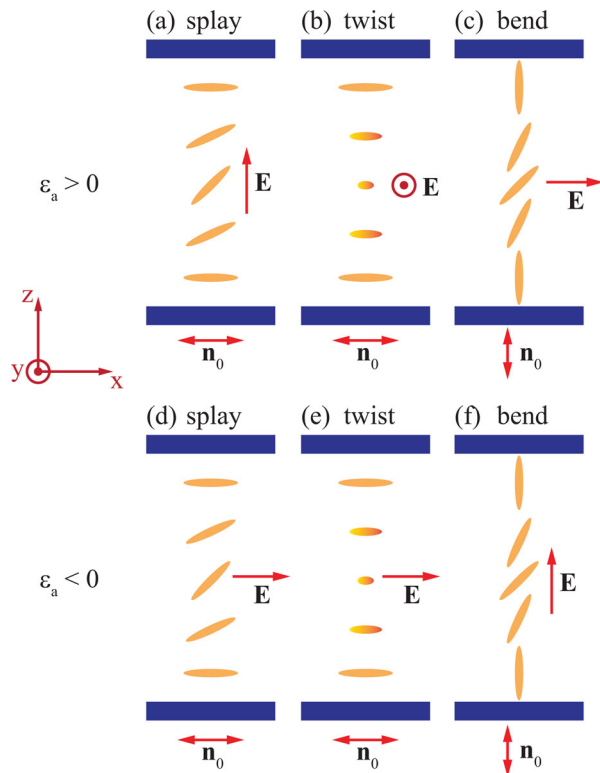


**Figure 1.** The frame of reference and sketches of the three main geometries (splay, twist and bend), where an electric field  $\mathbf{E}$  can induce a homogeneous deformation in a liquid crystal with (a)–(c) positive ( $\varepsilon_a > 0$ ) and (d)–(f) negative ( $\varepsilon_a < 0$ ) dielectric anisotropy.  $\odot$  indicates out-of-plane direction of  $\mathbf{E}$ . The double arrow indicates the initial director  $\mathbf{n}_0$ .

Which of those will be realised is determined by the combination of three sets of parameters. The first set depends on the geometry of the system and includes the initial director alignment  $\mathbf{n}_0$  and the cell thickness  $d$ . The second set contains the material parameters of the studied nematic. These include the dielectric permittivities ( $\varepsilon_{\perp}$  and  $\varepsilon_{\parallel}$ ), the electrical conductivities ( $\sigma_{\perp}$  and  $\sigma_{\parallel}$ ) and their anisotropies ( $\varepsilon_a = \varepsilon_{\parallel} - \varepsilon_{\perp}$  and  $\sigma_a = \sigma_{\parallel} - \sigma_{\perp}$ ), the three elastic constants ( $K_{11}$ ,  $K_{22}$ ,  $K_{33}$ ), the six viscosities ( $\alpha_1, \dots, \alpha_6$ ), the two flexoelectric coefficients ( $e_1$  and  $e_3$ ), etc. [1]. Finally, the third set specifies control parameters, i.e., the characteristics of the applied electric field by the magnitude of the applied voltage  $U$ , by its waveform (which can be a constant, sinusoidal, square wave, stochastic or their combination) and, in case of AC driving, by its frequency  $f$ . For sinusoidal signals, in the following, we will mean by  $U$  the root-mean-square (rms) value. The set of control parameters might include additional applied fields, e.g., a magnetic field or shearing.

The parameter combinations, where the system does not respond to the applied field [case (a) above], are important for those who want to avoid patterns. These include trivially the voltage ranges below the onset of patterns, but may involve also more complex situations (see, e.g., the case of ac + dc driving in Section 6.2). Case (b), in general, does not form part of pattern formation studies, except when non-equilibrium, transient scenarios involving flow occur during the onset of the deformation (see Section 2). It may also become relevant, if the presence of the homogeneous deformation is a prerequisite of pattern formation (see examples in Section 4.1.2). The main emphasis of this work will be paid to the great variety of patterns corresponding to the situation (c).

Patterns involve a spatial variation of the director (i.e., of the optical axis). Due to the transparency and the anisotropic optical properties of nematics, it can easily be observed by optical techniques. Variation of the tilt angle (the out-of-plane component) of the director changes the effective refractive index and, as a consequence, the birefringence of the sample. Commonly, the sample is placed between the crossed polarizers of a polarizing microscope (POM); then birefringence modulation appears as a variation of the intensity and/or the colour of the image [4]. In-plane (azimuthal) modulations of the director are also detectable with POM, though in this case, using circularly polarized light as illumination (i.e., inserting a  $\lambda/4$  plate in the light path) might improve the performance [5].

A spatially periodic refractive index modulation caused by director gradients behaves like an array of lenses, and periodically deflect the light path from the

incidence direction. The resulting focusing/defocusing effect leads to a spatial modulation of the transmitted intensity (in addition to that owing to the birefringence), called the shadowgraph image. The contribution of the birefringence can be eliminated if only a single polarizer (that ensuring illumination with extraordinary polarization) is used instead of the crossed ones. Moreover, the shadowgraph image is observable even without polarizer, though with lower contrast (as the light with ordinary polarization is fully transmitted). Tedious calculations of the light path through an inhomogeneous, anisotropic system concluded that sharp shadowgraph images can be obtained in three focal planes: when the microscope is focussed in the middle of the sample or to certain positions below and above it [6–8]. These focal positions are, however, not equivalent. The periodicity of the shadowgraph image matches that of the director field ( $\Lambda$ ) only, when focussed in the middle of the sample. For the other two positions, an apparent periodicity of  $\Lambda/2$  is observed.

Besides POM, light diffraction offers another possibility to observe and study patterns, as the periodic distortion is equivalent to an optical grating. The far-field diffracted image (which corresponds to the Fourier transform of the actual pattern) can be visualized on a screen and provides information, e.g., on the symmetry and the wave vector of the pattern.

All three optical techniques mentioned above are suitable to study the electric field-induced patterns. Which one is preferred depends on the actual pattern type. The snapshot images included in the present review were mostly (but not exclusively) prepared using the shadowgraph technique.

Besides the morphology and threshold behaviour, dynamics also belongs to the important characteristics of patterns. In order to analyse the dynamics of the phenomena driven by electric field, it is useful to list the typical relaxation times of the system: the director relaxation time  $\tau_d$ , the charge relaxation time  $\tau_q$  and the viscous relaxation time  $\tau_v$ , which are defined as

$$\tau_d = \frac{(\alpha_2 - \alpha_3)d^2}{K_{11}\pi^2}, \quad \tau_q = \frac{\varepsilon_0\varepsilon_\perp}{\sigma_\perp} \quad \text{and} \quad \tau_v = \frac{2\rho d^2}{\alpha_4}, \quad (1)$$

respectively ( $\varepsilon_0$  is the electric constant and  $\rho$  is the density).

Assuming a nematic with typical material parameters in a  $d = 20\text{-}\mu\text{m}$ -thick cell, one has  $\tau_d \sim 1\text{ s}$ ,  $\tau_q \sim 10^{-3}\text{ s}$  and  $\tau_v \sim 10^{-5}\text{ s}$ . These timescales play either dominant or negligible role, depending on their ratio to  $T = f^{-1}$ , the period of the applied AC electric field.

In the following sections, we attempt to give a non-exhaustive description of three main types of electric

field-induced patterns: the transients during the Fredericksz transition, the flexoelectric domains (FDs) and the electroconvection (EC).

## 2. Pattern formation during a Fredericksz transition

Fredericksz transition is commonly known as a field-induced uniform deformation resulting in a state distorted along  $z$ , but homogeneous in the plane of the sample [case (b) above]. More precisely, this statement applies to the final equilibrium state only, except when the external field is increased beyond its threshold value gradually, in very small steps (adiabatically slowly, to let the system continuously acquire its equilibrium state). If, however, the field is applied suddenly, in large steps, the system is driven out of equilibrium and forms transient patterns. Even in this case, the director configuration will reach the final equilibrium state (that corresponds to the destabilizing dielectric torque being compensated by the elastic torque) after a period of time, but during this time interval the system is out of equilibrium and reacts by developing a more or less ordered periodic, intermediate (transient) structure (Figure 2), which can be well characterized by a typical wave vector  $\mathbf{q}$  in the Fourier space. The coupling between inhomogeneous, time-varying director distribution and the fluid velocity produces shear flow, which lowers the effective rotational viscosity that explains the observed faster response of the spatially periodic state than that of the homogeneous distribution. The viscous effects are opposed by elastic forces, which become important when the wavelength reaches the order of the cell thickness.

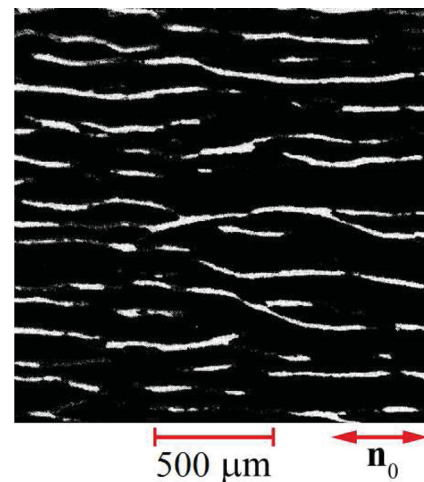


**Figure 2.** Snapshot of a transient pattern taken in the splay geometry on 5CB. The average wavelength is set by the cell thickness ( $d = 100\text{ }\mu\text{m}$ ) [9]. The double arrow indicates the initial director  $\mathbf{n}_0$ . Crossed polars; the light polarization is parallel to  $\mathbf{n}_0$ .

The first level of description involves the calculation of linear growth rates  $\nu(\mathbf{q})$  of individual Fourier components as a function of the wave number and finding the maximum of this quantity. The fastest growing wave number gives, in many cases, a reasonable description of the early stages of the pattern forming process, but the procedure must be mistrusted for two reasons: (i) the selectively amplified modes are initialized by thermal fluctuations, whose spectrum should be relevant and (ii) nonlinear effects may become important, or even decisive already at an early stage; thus, the homogeneous ( $q=0$ ) mode may be suppressed by nonlinear interactions with the  $q \neq 0$  modes.

Several experimental situations can be considered, depending on the geometry (splay, twist or bend configuration, see the typical Freedericksz geometries in Figure 1) and on the applied field: electric or magnetic. While in the equilibrium Freedericksz transition, the magnetically and electrically driven transitions are analogous, it is not the case when transient patterns occur.

In the *splay* geometry (Figure 1(a)), the wave vector of the magnetically driven stripes was predicted and found to be parallel [10,11] or slightly oblique [12,13] to the initial director  $x$ . On the contrary, in the electrically driven case, stripes are parallel with the director [9]. The differences arise from two sources: (1) as a result of anisotropic conductivity one has production of space charges and (2) the diamagnetic susceptibilities and their anisotropy are several orders of magnitude smaller than the dielectric permittivities. Consequently, the magnetic field remains homogeneous even in the distorted sample, while, on the contrary, in the electrically driven case, both effects (1) and (2) result in a nonuniform electric field in the Freedericksz-distorted state perpendicular to the director, which leads to transient stripes of very different properties from those observed in the same sample under magnetic field [14–16].

A three-dimensional (3D) *linear* stability analysis for the electrically driven case, including both effects (1) and (2), revealed that in the direction perpendicular to the director, the homogeneous mode is the fastest growing one here as well. A *weakly nonlinear* calculation, however, showed that, as a result of the two additional effects, a wave vector perpendicular to the initial director can also arise [15,16]. The theory also explains the experimentally observed crossover from perpendicular to parallel stripes, induced by changing the frequency of the electric field. The key feature is that the scenario is dominated by the conductivity effects at low frequency and by the dielectric permittivity at high frequencies. The two material parameters have several orders of magnitude difference, which makes the transition detectable.

In the *twist* geometry (Figure 1(b)), magnetically induced stripe structures, oriented perpendicular to the initial director alignment, were found [17–20]. Restricting the wave vector to the observed direction, i.e., within a two-dimensional (2D) description, the linear growth rates with realistic boundary conditions can be calculated analytically in this geometry. It describes the experiments quite well at early times. The coarsening observed at later times can be understood by nonlinear effects that were treated numerically using thermal noise as initial condition.

In the *bend* geometry (Figure 1(c)), the electric field-induced transition was studied in the presence of a competing magnetic field [21]. A periodic structure was found with a wave vector parallel to the planarly applied electric field. The stripes appeared to persist in low electric field, which is supported by a 2D calculation [22].

In all the above-mentioned geometries, the final equilibrium Freedericksz state is uniform. There are, however, situations when this is not the case. It has been shown theoretically that if the twist elastic constant  $K_{22}$  is extremely small compared to the splay ( $K_{11}$ ) and bend ( $K_{33}$ ) ones, a spatially periodic deformed state is preferred over the uniform one because of its lower free energy [23]. We are not aware that this theoretical possibility of an electric field-induced periodic twist Freedericksz transition has ever been justified experimentally. Its magnetic analogue has, however, been demonstrated [23] in a polymeric nematic system.

We note that the transient patterns described in this section are not the only 3D distortion types which may arise during the Freedericksz transition. The director tilt has a twofold degeneracy (tilt to the right or left are equivalent); the tilt direction is singled out accidentally at different locations. Domains of opposite tilt are separated by topological defects (Brochard–Leger walls, see, e.g., [24]) which disappear as time evolves, unless they are pinned at surface inhomogeneities or the cell boundaries. Although topological defects occur quite frequently in LCs and represent an interesting, growing field of LC science, they are not in the scope of the present review.

### 3. Flexodomains

Additional to the electric and elastic torques governing the Freedericksz transition, the flexoelectric torque is also present and cannot be neglected in some configurations; on the contrary, it becomes decisive and will itself be responsible for transitions into pattern forming states.

### 3.1. FDs driven by a DC field

By applying the same procedure as for describing the Freedericksz state, thus minimizing the free energy when adding to the electric and elastic contribution also the flexoelectric term, one can find a very regular, spatially periodic structure parallel to  $\mathbf{n}_0$  (parallel stripes along  $x$ ) above a threshold (see Figure 3(a)). The threshold voltage  $U_{FD}$  as well as the critical wave number  $q_{FD}$  can be calculated analytically in linear approximation of small director distortions and a condition for the formation of the pattern defines a constraint on the combination of material parameters [25]:

$$(e_1 - e_3)^2 > |\varepsilon_a| \varepsilon_0 K, \quad (2)$$

where  $K$  is the average elastic modulus.

This result has been obtained for rigid boundary conditions, for isotropic elasticity (one-constant approximation) and for a DC electric field. The structure that arises is due to the distortions of the basic director field, characterized by an out-of-plane tilt component  $n_z(y, z, t)$  and by an in-plane azimuthal component  $n_y(y, z, t)$ , both being periodic along  $y$  and depend on  $z$ :

$$\begin{aligned} n_x(y, z, t) &\approx 1; & n_y(y, z, t) &= \sin(py)\bar{n}_y(z, t) \ll 1; \\ n_z(y, z, t) &= \cos(py)\bar{n}_z(z, t) \ll 1. \end{aligned} \quad (3)$$

A review and summary of theoretical as well as experimental results has recently been given in [26].

The analysis has recently been extended to the case of anisotropic elasticity ( $K_{11} \neq K_{22} \neq K_{33}$ ) [27]. A transcendental equation was derived for the neutral curve  $U_0(q)$  at which the bifurcation from the basic planar state to flexodomains with wave number  $q$  takes place. A

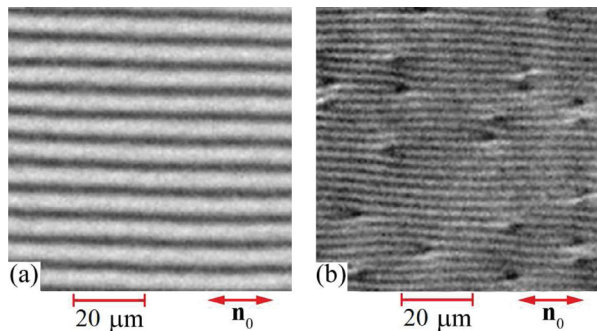


**Figure 3.** Snapshots of flexodomains in the BCN 2,5-bis(4-(difluoro(4-heptylphenyl)methoxy)phenyl)-1,3,4-oxadiazole (7P-CF2O-ODBP): (a) near onset, (b) much above onset ( $d = 6 \mu\text{m}$ ) (photos with courtesy of Y. Xiang). Shadowgraph images; the light polarization is parallel with  $\mathbf{n}_0$ .

relative elastic anisotropy

$$\delta k = \frac{K_{11} - K_{22}}{K_{11} + K_{22}} \quad (4)$$

was introduced, measuring the deviation of the system from the isotropic case, extending into both positive and negative directions. Solving the equation numerically for the neutral curve and minimizing it subsequently with respect to  $q$  yield the critical wave number and threshold voltage. As one of the most important results, the existence region of FDs was explored in the full range of material parameters [27]. The rigorous calculation showed that the director field in FDs and in the periodic splay-twist Freedericksz state [23] (mentioned in Section 2) is similar. The latter evolves, even in the absence of flexoelectricity, if  $\delta k$  is above a critical value.

A nonlinear analysis was also attempted [28] in order to predict the voltage dependence of the wavelength of FDs. Calculations could be performed only neglecting the boundary conditions (thus no  $z$ -dependence was assumed), which yielded  $U_c = 0$  and  $q \propto U$ . Indeed, experimentally a linear increase in the wave number with the applied voltage,  $q = q_c + \alpha(U - U_c)$ , was reported on different compounds [28–30]. The wavelength difference between FDs near to and far from onset can be clearly noticed by comparing Figure 3(a, b).

In view of the theoretical relation between the flexoefficients and  $q_c$ , observation of FDs offers a method for determining the combination  $|e_1 - e_3|$  by measuring the wavelength of FDs [31–33]. The advantage of this method is that there is no need to measure voltages, which may be problematic at low frequencies (see discussion in Section 5). Its disadvantage is that, unfortunately, the applicability of the method is restricted to those few compounds, which exhibit FDs.

A recent work [30] reported about the effect of a magnetic field on the formation and characteristics of FDs. The behaviour is complex and depends substantially on the relative orientation of the relevant fields: the  $\mathbf{E}$  electric, the  $\mathbf{H}$  magnetic and the  $\mathbf{n}_0$  director. Two geometries were studied experimentally as well as by numerical simulations. In the case of  $\mathbf{H} \parallel \mathbf{n}_0$ , the stabilizing effect of the magnetic field increases the FD threshold. If, however,  $\mathbf{H} \perp \mathbf{n}_0$ , the threshold voltage and critical wave number of FDs depend non-trivially (non-monotonically) on the magnetic field, exhibiting a minimum at  $H = H_F$ , at the magnetic twist Freedericksz threshold field. In addition, for  $H > H_F$ , the direction of the FDs rotates, following the director twist in the Freedericksz state. This rotation of  $\mathbf{q}$  may be regarded as a proof for the bulk origin of FDs. The magnetic field-induced reduction of the threshold voltage may allow the emergence of FDs in certain compounds, where no FDs are detectable at  $H = 0$ .

### 3.2. FDs driven by an AC field

The possibility of the formation of FDs at AC fields has already been examined in [25] and rigorously analysed and numerically tested in [27]. The calculation has been restricted to harmonic (sinusoidal) voltage with a given frequency  $f$ . Moreover, only very low frequencies compared with the inverse director relaxation time  $\tau_d$  have been taken into account, based on the experimental observations, which show that FDs can only be observed for very low  $f$ . At higher frequencies, for the available parameter ranges, either the equilibrium Freedericksz state or the very robust EC takes over which usually have lower threshold voltage. The crossover frequency between FDs and EC typically falls into the subhertz region.

The low-frequency range where  $f < 1/\tau_d$  involves specific phenomena, which are not present at DC driving and are negligible at higher  $f$ . When the period of the applied voltage is comparable or longer than  $\tau_d$ , the director distortion relaxes – partially or fully – within one period of the driving voltage towards its basic state. This leads to a non-stationary contrast; the pattern intensity fluctuates with the driving frequency. The flashing makes the experimental detection of the pattern characteristics more demanding than in the case of stationary contrast, but it can be handled. This specific phenomenon (flashing), which will be treated in more detail in Section 5, allows one to study different pattern forming phenomena: e.g., FDs and EC, which occur subsequently within one period of driving.

### 3.3. Flexodomains in bent-core nematics

Bent-core nematics (BCN) have several unusual properties compared with the calamitic nematics taken into account so far. The differences appear, e.g., in the ratio of elastic moduli, the order of magnitude of the viscosities and the flexoelectric coefficients [34]. Nevertheless, the pattern forming abilities under electric field are similar. Flexodomains as well as a variety of EC structures have been observed in planar as well as in twisted geometry.

In planar geometry, parallel stripes (wave vector is perpendicular to  $\mathbf{n}_0$ ) have been detected below 30 Hz on the substance 4-chloro-1,3-phenylene bis-4-[4'-(9-decenyloxy)benzoyloxy] benzoate (CIPbis10BB) in [35–37]. The pattern was interpreted differently, due to the much lower conductivity in the second experiment than in the first one. Stable longitudinal rolls have been seen on other bent-core nematics too [38,39].

Nonlinear field effects and defect dynamics were also studied [38], as well as special geometries like twisted cells [40].

## 4. EC

While for flexodomains the periodic director distortion (calculated from the principle of minimizing the free energy) alone provides a satisfactory description, there exists a long known phenomenon where, besides the director modulation, material flow and space charges play a just as important role in the pattern formation. This phenomenon is called EC; it is also known as the electro-hydrodynamic instability. Owing to the presence of flow, EC is a more complex phenomenon, which has an inherently dissipative character. Depending on the sample's properties and the driving conditions, a multitude of pattern morphologies may be formed. These mostly include stripe patterns with a diverse range regarding the wavelength and the direction of the stripes, but two-dimensional (square grid or hexagonal) patterns, localized deformations (worms, Maltese crosses, dendrites and fingers) as well as complex structures (chevrons, wavy pattern, CRAZY rolls and spirals) involving topological defects (dislocations or disclinations) have also been reported. Representative images will be shown later during the detailed discussions. Based on the cumulated experiences and some theoretical considerations, one could deduce that the signs of the dielectric and the conductivity anisotropies are especially important in deciding what kind of EC patterns can exist in a nematic if any [41]. Therefore, it is convenient to classify LCs into groups of various sign combinations of  $(\text{sgn}(\varepsilon_a) \text{sgn}(\sigma_a))$  [1,42]; e.g.,  $(-+)$  meaning  $\varepsilon_a < 0$ ,  $\sigma_a > 0$ .

The expanding richness of the patterns and the complexity of the mechanisms behind them have justified reviewing EC from time to time, from different aspects, marking the way for gradually understanding the phenomenon: introducing various pattern types and presenting only simple models [2,43,44], providing thorough theoretical overviews with approximate analytical formulas [45–47], discussing the role of anisotropies [41], addressing the importance of alignment symmetries [48] and the role of flexoelectricity [31] in pattern formation.

### 4.1. The standard model of EC and its extensions

A classical example of EC, the Williams domains [49], is observable in a thin layer of planarly aligned  $(-+)$  nematic, which is subjected to a DC or an AC (rms) voltage  $U$ , resulting in an electric field  $\mathbf{E}$  perpendicular to the substrates. While the initial, homogeneous state is preserved if the applied voltage is low, it becomes unstable towards distortions when  $U$  exceeds a critical

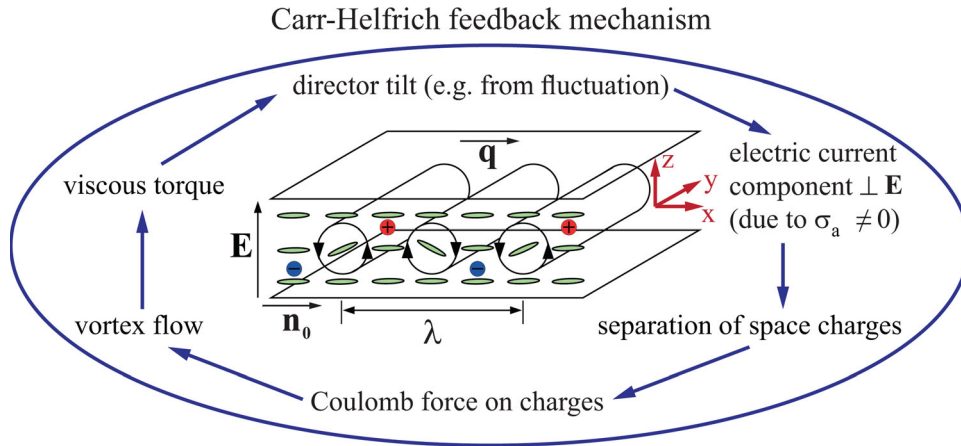


**Figure 4.** Illustration for the Carr–Helfrich feedback mechanism. Green rods represent the nematic director, black circles with arrows indicate the flow directions, the red and blue bullets mark the + and – space charge clouds, respectively.

(threshold) value  $U_c$ . As nematic LCs are optically uniaxial materials, the periodic tilt (out-of-plane) distortions of the director yield a modulation of the refractive index, which makes the pattern visible in a polarizing microscope as a sequence of dark and bright stripes; either due to birefringence when using crossed polarizers or owing to focussing/defocussing effects (shadowgraph technique [6–8]) if using single or no polarizer. The occurrence of the instability can be understood via the fundamental Carr–Helfrich (C–H) feedback mechanism (named after its discoverers [50,51]), illustrated in Figure 4.

Infinitesimal, spatial director tilt modulations may always be present in a planar nematic due to thermal fluctuations. The director field is subjected to elastic and dielectric restoring torques. However, due to tilt and to  $\sigma_a \neq 0$ , the electric current has a nonzero component perpendicular to  $\mathbf{E}$ , which leads to a space charge formation. Owing to the Coulomb force acting on the charges, a material flow is induced. Being confined by the substrates, the flow forms vortices, which exert a destabilizing viscous torque on the director; thus closing the feedback loop. For  $U < U_c$ , the feedback is negative and the director fluctuations decay. However, for  $U > U_c$ , the feedback becomes positive for one Fourier mode of the fluctuation with a critical wave vector  $\mathbf{q}_c = (q_c, p_c, 0)$ , which thus grows to a pattern of finite amplitude.

If one would like to calculate or predict the characteristics of EC patterns, the inestimable ideas above have to be converted into the form of differential equations. The comprehensive theoretical model, capable of describing the formation of various EC pattern morphologies, has been developed during decades and is now referred to as the standard model (SM) [52]. The model combines the equations of nematodynamics (for director relaxation and flow) with Maxwell’s equations, assuming that nematics are incompressible, have a finite (small)

ohmic electrical conductivity and flexoelectricity is negligible. It finally provides a set of six coupled nonlinear partial differential equations (PDEs) for the six independent variables: two components of the director field  $\mathbf{n}(\mathbf{r})$ , the velocity field  $\mathbf{v}(\mathbf{r})$  and the electric potential  $\phi(\mathbf{r})$ . As boundary conditions at the substrates, strong director anchoring, no-slip condition for the velocities and no charge transfer through the electrodes are assumed.

Unfortunately, the complexity of these equations does not allow fully analytical solutions; thus further approximations are required in order to draw specific conclusions on pattern characteristics. The most obvious assumption is that at the onset of the instability, the pattern amplitude (e.g., the maximum director tilt) is small. It holds if the amplitude grows continuously from zero with the voltage rising above  $U_c$  (forward bifurcation), which condition fulfils, by fortune, for most EC patterns. Then nonlinear terms in the PDEs can be neglected and a linear stability analysis of the initial state can be performed [53]. Separating the spatially periodic ( $e^{i\mathbf{q}\cdot\mathbf{r}}$ ) and an exponentially growing ( $e^{\nu t}$ ) part of the variables from the remaining  $z$  and  $t$  dependence, which are expressed by truncated Fourier series, the PDEs can be converted to a set of algebraic equations for the Fourier coefficients. The growth rate  $\nu(\mathbf{q}, U)$  is obtained from the solubility criterion. Finally, the  $\nu(\mathbf{q}, U) = 0$  condition defines a  $U(\mathbf{q})$  neutral surface, whose minimum  $U_c(\mathbf{q}_c)$  provides the onset voltage  $U_c$  and the critical wave number  $\mathbf{q}_c$  of the pattern.

The procedure above can be applied in the case of DC driving ( $U = U_{dc}$ ), as well as for AC excitations ( $U = U_{ac}\sqrt{2} \sin 2\pi ft$ ) in a wide range of frequencies  $f$ . For the latter case, inspection of the SM equations shows that they can have two solutions with different time symmetries. In the so-called *conductive regime* ( $\langle n_z \rangle \neq 0$  ( $n_z$  has the same sign in both half periods)), while in the *dielectric*

regime  $\langle n_z \rangle = 0$  ( $n_z$  changes its sign in subsequent half periods). This latter is the only solution if  $f$  is higher than the so-called *cut-off* frequency  $f_{\text{cut}}$  which is related to  $\tau_q$ . Here,  $\langle \rangle$  corresponds to the time average over a driving period. This practically means that, in leading order, the director tilt (and the flow velocity) modulation in conductive EC patterns is stationary, whereas the space charges oscillate with the driving frequency; in the dielectric regime, on the contrary, the director and the flow oscillates, but the space charge pattern becomes stationary.

Approximate analytical formulas can be obtained, if only the leading terms of the Fourier series (in  $z$  and  $t$ ) are kept [45]; for more precise  $U_c$  and  $\mathbf{q}_c$  values, numerical methods are needed, which require the knowledge of a complete set of material parameters (listed in Section 1). The SM is able to explain experimental results on EC pattern formation for a large group of nematics [(−+) and (+−) materials] qualitatively and, when the material parameters are known to high enough precision, also quantitatively. These EC phenomena, which are thus explicable with the SM, have been denominated as *standard electroconvection* (s-EC) and will be discussed in Sections 4.1.1 and 4.1.2 in more detail. In other groups of nematics, which have a different combination of material parameters [(−−) and (++) materials], however, no instability should occur according to the SM; EC patterns have, nevertheless, been observed occasionally even in those materials. These phenomena, which cannot be accounted for by the SM, are known as *nonstandard electroconvection* (ns-EC) and will be addressed in Section 4.2.

The linear stability analysis has an unimpeachable role in determining the onset characteristics of the pattern, the  $z$ -profile of the variables as well as the mutual relations between the magnitudes of the director components, the velocities and the space charges. By neglecting the nonlinear terms, it fails, however, to provide information about how the pattern amplitude  $A$  depends on the applied voltage. The nonlinear features just above the onset (weakly nonlinear description) can be handled by the amplitude formalism, using Ginzburg–Landau equations (GLEs) that may couple the amplitude (and the azimuthal angle of the director) with the voltage [53]. Here, a critical task is the calculation of the coefficients of the GLEs from the raw PDEs. In return, not only the  $A(U)$  relation, but also certain morphological transitions can be predicted (see also Section 4.3).

The existence of ns-EC patterns clearly shows that, though the SM includes essential ingredients of the pattern formation process, it does not provide a complete description. Further development of the theory requires the incorporation of additional effects, originally

neglected in the SM. One example is the extended SM, which incorporates flexoelectricity by adding a few new terms into the existing set of PDEs. These extended equations are listed in the appendix of Ref. [54]. Its importance will be made clear in Sections 4.1.1 and 4.2.

Although ohmic conductivity of LCs is a basic assumption of the SM, this is clearly a simplification. The conductivity of LCs originates in the ionic contaminants; consequently, ionic effects should be taken into account in a more complete description. This has, at least partially, been done by introducing the weak electrolyte model (WEM) [55], which can handle charge carriers (ions) of opposite charge as well as the association, dissociation and migration of ions. Thus, the WEM has a great scientific potential in explaining EC phenomena; unfortunately, on the expense of increasing the number of governing equations, introducing new timescales and requiring the knowledge of further (not easily measurable) material parameters. So far, the WEM has only been analysed from one aspect: it has explained the Hopf bifurcation at EC onset (which cannot be obtained in the frame of the SM); thus explained the nature of the travelling waves in s-EC (see also Section 4.1.1).

#### 4.1.1. EC as a primary instability

Most of the materials that exhibit s-EC belong to the (−+) group; they include single compounds such as *p*-azoxyanisole (PAA) [49], *n*-4'-methoxybenzylidene-*n*-butylanilin (MBBA) [56], 4-ethyl-2-fluoro-4-*c*-[2-(trans-4-pentylcyclohexyl)-ethyl] biphenyl (I52) [57] or 4-*n*-octyloxy-phenyl 4-*n*-methoxybenzoate (1008) [32], as well as mixtures such as Phase 4 [58], Phase 5/5A (Merck) [59,60] or Mischung 5 [61]. For decades, the majority of experiments (and thus also the related theoretical simulations) have been performed at AC excitation with  $f$  being in the audio frequency range. Under such conditions, the period time  $T = 1/f$  of the driving voltage is much shorter than the director relaxation time  $\tau_d$  or the growth/decay times of the pattern, which depends besides  $\tau_d$  on the wavenumber [62] and on the excess voltage  $\Delta U = U - U_c$  [63,64] too. Thus, several cycles are required for the stabilization of the pattern. The other limit,  $T > \tau_d$ , will be discussed later in Section 5.

In planar samples of (−+) materials, EC is a primary instability: upon increasing the voltage, the pattern emerges directly from the homogeneous initial state. It is composed of convection rolls, which appear in the microscope as a sequence of stripes with different intensity (or colour).

It follows from the SM (Section 4.1) that (−+) compounds have two EC regimes with distinct temporal dynamics; both might exist for  $f < f_{\text{cut}}$ . The onset characteristics, i.e., the frequency dependence of the

threshold voltages  $U_c(f)$  and of the wave vectors  $\mathbf{q}_c(f)$ , are different in the two regimes. At lower frequencies, in the conductive regime,  $U_c(f)$  increases steeply with  $f$  exhibiting a divergence-like behaviour. At higher  $f$ , in the dielectric regime, the frequency dependence of the threshold is weaker,  $U_c(f) \propto \sqrt{f}$ . Consequently, there is a crossover frequency  $f_c$ , where the  $U_c(f)$  curves intersect. This crossover frequency is typically at about 60–80% of  $f_{cut}$ . For  $f < f_c$ , conductive rolls (Figure 5(a,b)), while for  $f > f_c$ , dielectric rolls (Figure 5(c,d)) have lower threshold (see Figure 6); therefore, by increasing the frequency, a crossover from conductive to dielectric rolls occurs. This transition is easily perceptible via the jump in the pattern wavelength: in the conductive regime,  $\lambda$  is about the sample thickness  $d$ , while in the dielectric regime, the wavelength is defined by a combination of the material parameters and is independent of the thickness; if  $d$  falls in the usual range of 10–100  $\mu\text{m}$ ,  $\lambda$  of the dielectric pattern (typically 3–4  $\mu\text{m}$ ) is much smaller than that of the conductive one. At  $f = f_c$ , the two patterns may coexist, either side by side or superposed [65].

At the crossover, the temporal dynamics of the pattern also changes. Although the difference in the temporal evolution within the driving period cannot be perceived by the naked eye when  $f$  is in the audio frequency range, it

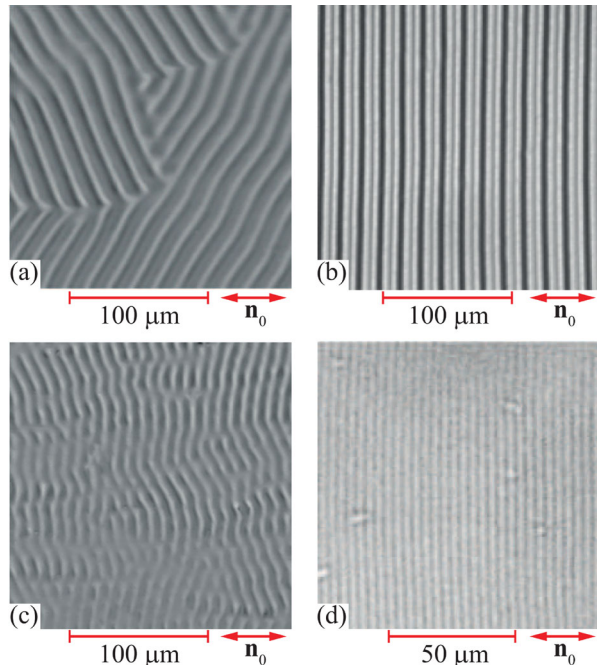


**Figure 5.** Snapshots of s-EC patterns in planar (– +) samples near onset: (a) conductive oblique rolls (1008,  $d = 11 \mu\text{m}$ ), (b) conductive normal rolls (Phase 5,  $d = 12 \mu\text{m}$ ), (c) dielectric oblique rolls (1008,  $d = 11 \mu\text{m}$ ) and (d) dielectric normal rolls (Phase 5,  $d = 11.4 \mu\text{m}$ ). The double arrows indicate the initial director  $\mathbf{n}_0$ . Shadowgraph images; the light polarization is parallel with  $\mathbf{n}_0$ .

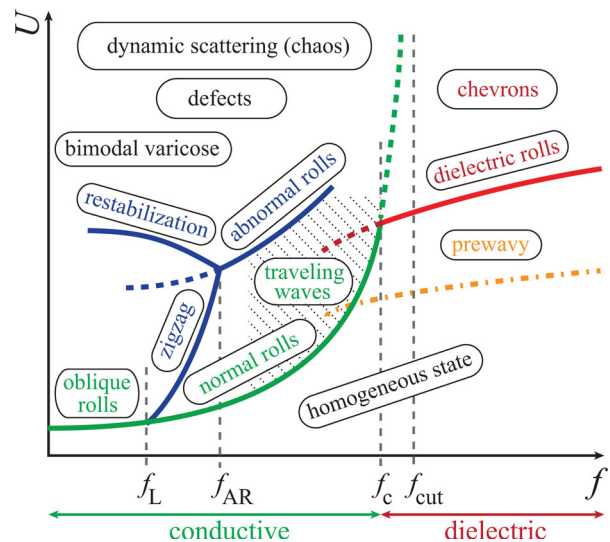


**Figure 6.** A typical schematic morphological phase diagram (the frequency dependence of the onset voltage of patterns) for planar (– +) nematics.

could be detected by using fast cameras for image recording [61,65] or by monitoring the intensity of the light diffracted by the patterns [66].

The convection rolls are oriented either perpendicular to the initial director alignment (normal rolls, NR,  $\mathbf{q} \parallel \mathbf{n}_0$ , Figure 5(b,d)) or are slightly rotated by an angle  $\alpha$  with respect to this direction (oblique rolls, OR, Figures 5(a,c)). In the latter case, the two possible rotation directions are degenerate, which often leads to zigzag structures. Usually, OR is observed at low frequencies; increasing  $f$ , the obliqueness angle  $\alpha$  decreases monotonically, roughly following the relation  $\alpha \propto \sqrt{f_L - f}$ . At the Lifshitz point  $f_L$ , there is a crossover from oblique to normal rolls ( $\alpha$  becomes zero). It has to be emphasized that the crossover between the conductive and dielectric regimes (involving the change of  $|\mathbf{q}|$ ) is not related to the crossover between OR and NR;  $f_c$  and  $f_L$  depend on different combinations of the material parameters. Therefore, even though the Lifshitz point has been found almost exclusively to fall into the frequency range of the conductive regime (as it is shown, e.g., in the schematic morphological phase diagram in Figure 6), resulting in conductive OR to conductive NR transition, it need not be so. Indeed, recently a crossover from dielectric OR to dielectric NR in Phase 4 [58], as well as a sequence of conductive OR – dielectric OR – dielectric NR transitions in the nematic 1008 [32], has also been reported.

The  $U_c(f)$  and  $\mathbf{q}_c(f)$  dependences calculated from the SM for both EC regimes are in good agreement with the experimental observations summarized above. The matching between experimental data and the theoretical predictions can further be improved by using the

extended SM, which can take into account the influence of flexoelectricity [54,67]. While it does not affect significantly the onset characteristics in the conductive regime, it reduces the dielectric threshold by about 30% [27].

Figure 6 shows a hatched area, which needs a special attention. In certain cases, there is a frequency range in the conductive regime close to  $f_c$ , where the roll pattern at onset is not stationary; instead, it is travelling in both directions normal to the rolls [68,69]. Whether *travelling waves* exist, depends on the material as well as on the sample thickness. If they are present, the lowest frequency where they appear is independent of the Lifshitz point; thus travelling OR and NR patterns have equally been reported. Travelling waves are an experimental manifestation of the Hopf bifurcation (the growth rate of the pattern has an imaginary part too). As we already mentioned in Section 4.1, the travelling feature of these patterns cannot be reproduced by the (extended) SM; the interpretation requires incorporation of ionic effects as it was done in the weak electrolyte model [55]. The predictions of the WEM for the Hopf frequency (which determines the travelling speed) have been experimentally justified in two nematics, I52 [57] and Phase 5A [70,71]. Interestingly, the  $U_c(f)$  and  $q_c(f)$  onset characteristics calculated from the WEM for travelling waves differ only very little from the values provided by the much simpler SM. This is the reason why travelling waves in  $(- +)$  compounds are still categorized as s-EC.

We should mention that the fast development of alignment technologies allows one to prepare much more complex geometries than a simple planar cell. Recently, studies on a planar-periodic sample have been reported, where one substrate is unidirectionally aligned, but on the other one the director, though planar, rotates periodically when moving along the  $x$ -direction [72]. As a result, there is a periodical twist deformation in the sample with domains separated by disclination lines. Using MBBA, two different EC scenarios were observed, depending on the sample thickness. At large  $d$ , the twist had no influence on the conductive EC rolls. At low  $d$ , however, the twist deformation made the normal rolls curved.

Theoretical calculations have been performed for another sophisticated geometry, where the sample thickness varies in a direction perpendicular to  $\mathbf{n}_0$  [73]. Emergence of stable patterns with branching rolls is predicted; experimental verification is still awaited.

So far all theoretical results and experimental observations were referred to cells of large aspect ratio (nearly infinite sample). Reducing the aspect ratio (i.e., reducing the electrode size) requires additional considerations, as then the lateral boundary conditions become non-negligible. This affects the wavelength selection

mechanism: an integer number of wavelengths should fit into the active area [74–77].

Side-view cells represent a different,  $90^\circ$  rotated geometry with a lateral electric field, to be used for exploring and visualizing the convection patterns in the plane parallel to  $\mathbf{E}$  [78–80]. This geometry corresponds to a very low aspect ratio in one direction; therefore, it is unclear to what extent do the identified convection profiles agree with those present in usual, high aspect ratio samples. Nevertheless, in the conduction regime, convection was found to fill the space between the electrodes; in the dielectric regime, it was rather concentrated to the region near the electrodes [80]. This observation agrees with the findings on EC in twisted nematic cells [81].

Although planar  $(- +)$  samples are the paradigm of s-EC, it is easy to see that the C–H mechanism works also in homeotropic  $(+ -)$  samples [1]. From theoretical point of view, there is, however, a principal symmetry difference between the two cases. In planar  $(- +)$  materials, there is a preferred direction in the plane of the substrates, thus the initial state is anisotropic in the plane of the sample, in two dimensions (2D). In contrast to this, in homeotropic  $(+ -)$  samples, the director is normal to the substrates, i.e., all directions parallel to the substrates are equivalent; hence, the initial state is isotropic in 2D. It means that the anisotropic patterned state emerges directly from the isotropic initial one and, as a consequence, the patterns developing are not expected to be ordered. Experimental studies on this kind of pattern formation are scarce as, unfortunately, nematics belonging to the  $(+ -)$  group are very rare. Systematic observations were made on an exotic, swallow-tailed compound, which exhibited disordered oblique (zigzag) rolls (Figure 7(a)) at lower  $f$ , which cross over to long-wave-modulated *square grid patterns (soft squares)* (Figure 7(b)) above a critical frequency  $f^*$  [82]. These pattern morphologies could be reproduced via simulations based on the SM. Very recently a calamitic mixture offering similar scenarios was also reported [83].

#### 4.1.2. EC as a secondary instability (homeotropic)

In homeotropic  $(- +)$  nematics, the Carr–Helfrich mechanism does not produce a destabilizing torque; therefore, in this geometry, no direct transition from the initial state to EC is possible. The negative dielectric anisotropy, however, leads to a bend Freedericksz transition (as a first instability, Figure 1(f)) resulting in a quasiplanar state (which is homogeneous in the  $x$ – $y$  plane, but is distorted along  $z$ ), where the C–H mechanism becomes effective again. Thus, EC may set in at voltages exceeding the Freedericksz threshold  $U_F$ , as a secondary instability [84]. For theoretical modelling, one can follow the procedure outlined in Section 4.1,

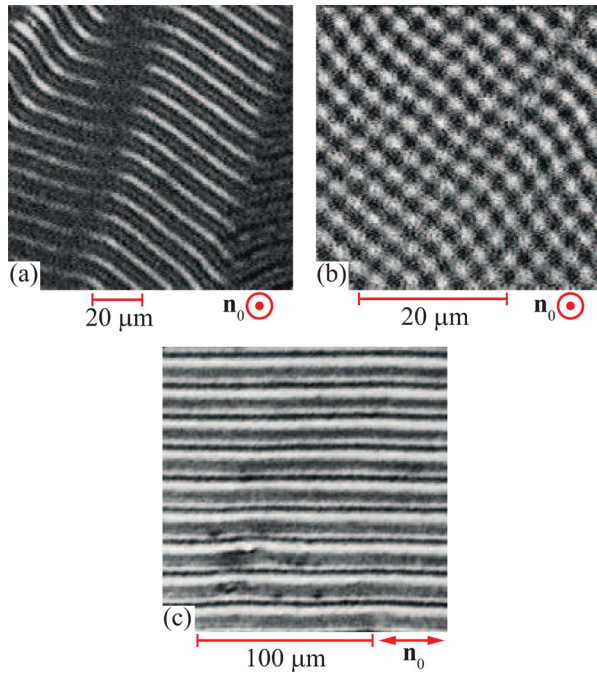


**Figure 7.** Snapshots of s-EC patterns in a (+ -) swallow-tail nematic compound near onset: (a) disordered rolls, (b) soft squares in a homeotropic sample ( $d = 11 \mu\text{m}$ ) and (c) parallel rolls in a planar sample ( $d = 11 \mu\text{m}$ ) [82].  $\odot$  and  $\leftrightarrow$  indicate out-of-plane and in-plane directions of  $\mathbf{n}_0$ , respectively. Shadowgraph images; the light polarization is horizontal.

though it becomes more tedious, as now the stability of an already distorted Fredericksz state should be checked against periodic modulations [85]. The exhibited pattern morphologies and frequency-induced crossover scenarios are the same as those for the planar samples outlined in Section 4.1.1: conductive and dielectric regimes, oblique (Figure 8(a,b)) and normal (Figure 8(c,d)) rolls can be detected as well. Thus, Figure 6 may serve as a schematic morphological diagram also for homeotropic (- +) nematics with one correction: one should add a horizontal line for the frequency-independent Fredericksz threshold lying below all EC curves.

Under some, not yet fully specified conditions, which are met by Phase 5A (but not met by MBBA), however, homeotropic samples may exhibit some unusual features. It was shown by experiment as well as by simulation that homeotropic Phase 5A has two Lifshitz points: it has NR at low as well as at high frequencies, and OR in between [86].

Although the initial, homeotropic state is isotropic in 2D, this symmetry breaks during the Fredericksz transition; thus, in contrast to the homeotropic (+ -) case above in Section 4.1.1, the patterns appear already on an anisotropic background. The azimuthal direction of the tilt is, however, singled out during the Fredericksz transition accidentally; it is a soft mode, the azimuthal

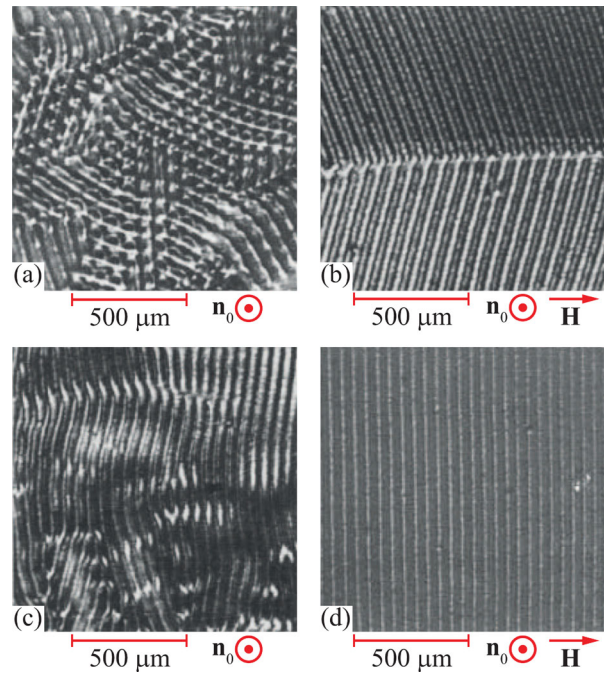


**Figure 8.** Snapshots of s-EC patterns in homeotropic MBBA ( $d = 50 \mu\text{m}$ ): (a) disordered conductive oblique rolls, (b) conductive oblique rolls ordered by an in-plane magnetic field  $\mathbf{H}$ , (c) disordered conductive normal rolls and (d) conductive normal rolls ordered by an in-plane magnetic field  $\mathbf{H}$ . The initial director  $\mathbf{n}_0$  is normal to the image plane. Shadowgraph images; the light polarization is horizontal.

angle varies in space and time. Consequently, the EC patterns are also disordered, chaotic (see Figure 8(a,c)). This kind of pattern formation is an example of a direct transition to spatiotemporal chaos [87]; it is also called soft mode turbulence (SMT) [88]. This phenomenon attracted lot of interest from both theoretical and experimental point of view; its extensive literature cannot be reviewed here.

The azimuthal degeneracy originating in the homeotropic alignment can be lifted by applying a small magnetic field  $\mathbf{H}$  parallel to the substrates [89,90]. Theoretically, an infinitesimal  $\mathbf{H}$  would be sufficient to break the degeneracy and introduce a preferred direction parallel with  $\mathbf{H}$ ; experimentally,  $H$  equal to about the third of the Fredericksz threshold field  $H_F$  might be needed to safely overcome accidental alignment imperfections and to order the EC patterns (see Figure 8(b,d)). Switching on-off a static magnetic field [91] or using an AC magnetic field [92], the dynamics of the SMT regime could be studied.

Planar (+ -) nematics are another example of s-EC occurring as a secondary instability. Here, a splay Fredericksz transition is induced by the applied voltage first (Figure 1(a)), then EC can emerge from the Fredericksz-distorted, quasihomeotropic state at

higher voltages. In contrast to the 2D isotropy of homeotropic (+ −) samples, this quasihomeotropic state is anisotropic. Thus, well-ordered roll patterns have been detected, however, with the roll direction parallel to the initial orientation (Figure 7(c)), in a swallow-tailed compound [82]. As other representatives of (+ −) nematics, an LC dimer composed of a calamitic and a bent-core molecule [93,94] as well as a calamitic mixture [83] were also tested and pattern sequences of longitudinal rolls–oblique rolls–normal rolls were detected upon increasing the frequency.

#### 4.2. Nonstandard electroconvection

The existence of standard EC relies on whether the C–H mechanism can provide a destabilizing torque on the director. It can be seen that if, in the geometry of Figure 4, the sign of  $\sigma_a$  alters, yielding (− −), the polarity of the space charges and thus the directions of the flow and of the viscous torque also change to the opposite. Therefore, the feedback remains negative and director fluctuations decay for all voltages; thus, no pattern should arise according to the SM. In contrast to this prediction, however, it has been known for a long time that some planar samples of the (− −) group of nematics, e.g., *n*-(*p*-*n*-butoxybenzylidene)-*n*-octylanilin (4O.8) [95,96], di-*n*-4-4'-octyloxyazoxybenzene (C8) [95], 4-*n*-decyloxyphenyl-4-*n*'-hexyloxy-benzoate (10/6) [42] and 4-*n*-octyloxy-phenyl-4-*n*'-heptyloxy-benzoate (8/7) [42,97], do exhibit EC upon voltage excitation. The assortment of compounds suitable for studying this type of ns-EC is quite narrow; they usually have a smectic (preferably smectic C) phase below the nematic one in order to have  $\sigma_a < 0$  in the lower temperature part of the nematic range. A common feature of the patterns is that they are *longitudinal rolls* (running parallel [Figure 9(a)] or at small angles [Figure 9(b)] to the initial director); they

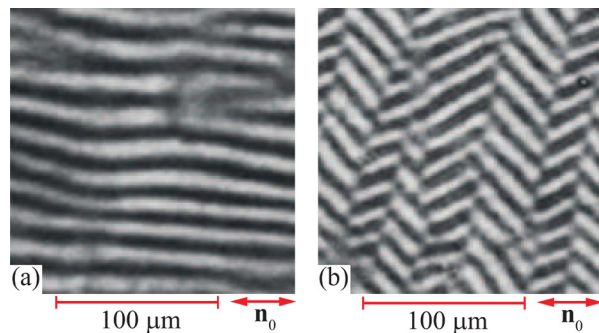


**Figure 9.** Snapshots of ns-EC patterns taken with nearly crossed polarizers in a planar (− −) sample (8/7,  $d = 12 \mu\text{m}$ ): (a) longitudinal rolls and (b) oblique rolls. The double arrows indicate the initial director  $\mathbf{n}_0$ .

have low contrast, are best visible at nearly crossed polarizers; moreover, the rolls are much less ordered than those of s-EC. They are typically observable in a limited (low) frequency range and have a linear  $U_c(f)$  dependence.

Although the SM cannot account for this instability, it has been shown recently that incorporating flexoelectricity into the SM (i.e., using the extended SM) already does the job [54]. The flexoelectric polarization arising due to a periodic director distortion with  $\mathbf{q} \perp \mathbf{n}_0$  creates a space charge modulation of opposite sign compared to that caused by the conductivity anisotropy. This dominance of the flexoelectric charges makes the feedback loop positive and leads to the appearance of the longitudinal rolls of the ns-EC as a primary instability in planar samples. In contrast, in homeotropic samples of the same materials, the patterns may appear only as a secondary instability, following the bend Freedericksz transition (Figure 1(f)).

It is worth noting that the flexoelectric terms in the PDEs provide some coupling between solutions of the conductive and of the dielectric types with different  $z$ -profiles; nevertheless, the latter are dominating [54]. Indeed, in experiments, the contrast (and also the diffraction intensity) of ns-EC longitudinal rolls was found to oscillate with the excitation frequency [66].

Occasionally, longitudinal rolls can also be travelling [97], indicating that Hopf bifurcation may exist in ns-EC. The measured Hopf frequencies seem to follow a similar functional dependence as that in s-EC. It is anticipated that the combination of the WEM with flexoelectricity could provide a full interpretation of the observations.

Nematics of (+ +) type are another group of materials where the SM does not predict patterns, yet ns-EC has been observed. A representative of this group is the well-known 4-cyano-4'-pentylbiphenyl (5CB), where homeotropic samples exhibited a direct transition to ns-EC yielding a low contrast 2D cellular pattern (Figure 10(a)) [98,99], which, under special conditions, could have hexagonal symmetry [100]). In planar samples of 5CB, ns-EC was also observed (Figure 10(c)), however, only at voltages above the splay Freedericksz threshold (Figure 1(a)), as a secondary instability. Roll patterns (disordered, fingerprint-like [Figure 10(b)] for homeotropic, ordered normal rolls [Figure 10(d)] for planar samples) were also seen at much higher voltages [99]. In 5CB [101] and in similar, highly polar compounds such as *p*-octyl-*p*'-cyanobiphenyl (8CB) [102,103], *p*-cyanobenzylidene-*p*'-octyloxyaniline (CBOOA) [102], 4-*n*-octyloxy-4'-cyanobiphenyl (8OCB) [103] or mixtures [102,104], an additional pattern morphology, a swarm of Maltese crosses (Figure 11), presumably corresponding to circular domains, could also be seen.

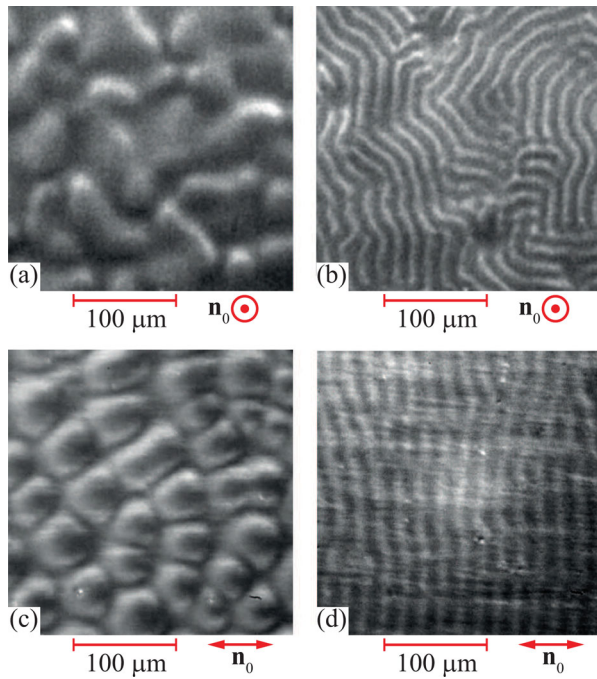


**Figure 10.** Snapshots of ns-EC patterns taken with nearly crossed polarizers in (+ +) samples: (a) cellular pattern at onset, (b) disordered rolls at high voltage in homeotropic 5CB ( $d \approx 30 \mu\text{m}$ ), (c) cellular pattern at onset and (d) normal rolls at high voltage in planar 5CB ( $d \approx 20 \mu\text{m}$ ) [99].  $\odot$  and  $\leftrightarrow$  indicate out-of-plane and in-plane directions of  $\mathbf{n}_0$ , respectively.

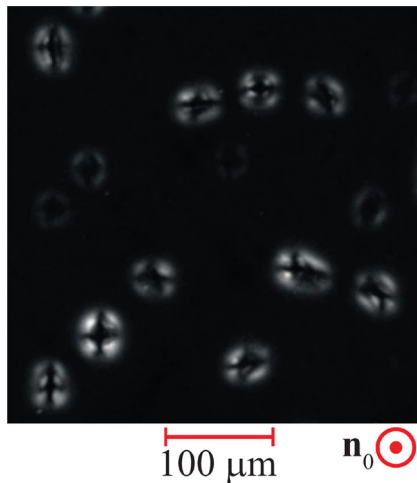


**Figure 11.** Localized ns-EC pattern in a (+ +) sample: Maltese crosses, presumably corresponding to circular domains in homeotropic 5CB ( $d = 50 \mu\text{m}$ ).  $\odot$  indicates the out-of-plane direction of  $\mathbf{n}_0$ . Crossed polarizers; the light polarization is horizontal.

Note that the occurrence of ns-EC in those compounds is especially surprising, in view of the large stabilizing torque due to the large ( $\epsilon_a \sim 9$ ) dielectric anisotropy. In the homeotropic alignment, flexoelectricity does not have a destabilizing effect; so even the extended SM fails to explain these observations. Some

authors have proposed the Felici–Bénard isotropic mechanism (related to charge injection through the electrodes, not based on the anisotropy of LCs) as a reason for these instabilities [102,104,105]; unfortunately, its rigorous theoretical description capable for predicting the onset characteristics of the patterns has not yet been developed. We anticipate that the equations of the WEM [55] contain, in principle, all necessary contributions. Nevertheless, a precise analysis of the problem using the WEM will be a very challenging task for theoreticians.

The above ns-EC patterns occur in groups of nematics characterized by specific combinations of their material parameters. There is, however, a structure called *prewavy* (PW) pattern [56,106–108] (also known as wide domains), which does not seem to have this restriction; it has been observed in (– +) as well as in (– –) materials. The prewavy pattern (Figure 12(a)) consists of stripes running perpendicular to the initial director with a wavelength much larger than  $d$ , which are visible with crossed polarizers only. They have a slow dynamics with the growth/decay times in the order of minutes. In the neighbouring stripes, the director has azimuthal angles of opposite sign and there is a flow along the stripes (parallel to the substrates) in opposite directions [108]. In calamitics, it is typically detectable at high frequencies

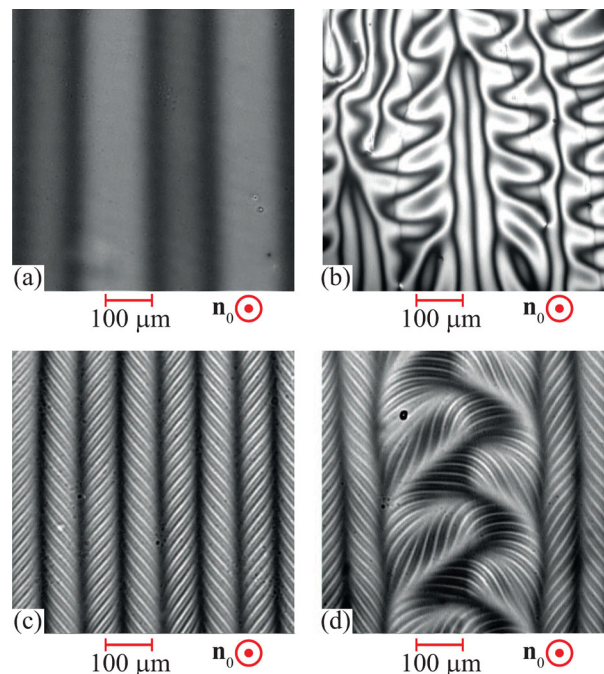


**Figure 12.** Snapshots of ns-EC patterns in homeotropic MBBA ( $d = 50 \mu\text{m}$ ): (a) prewavy pattern, (b) wavy pattern, (c) defect free chevrons (superposition of the prewavy pattern with normal rolls), (d) superposition of the wavy pattern with normal rolls.  $\odot$  indicates out-of-plane direction of  $\mathbf{n}_0$ , the direction of the Freedericksz-tilt is horizontal. Crossed polarizers; the light polarization is horizontal.

with a weak, nearly linear frequency dependence of the thresholds. Namely, a crossover from conductive rolls to PW was reported in MBBA [107] and Phase 5A [109] (the dash-dotted line in Figure 6 illustrates this scenario), but a sequence of conductive rolls – dielectric rolls – PW pattern can also occur [109]. PWs were observed in the nematic 4,*n*-heptyloxybenzoic acid (7OBA) too [110,111]. Recently, it has been proven that the pattern exists even in the vicinity of the nematic-to-isotropic phase transition [112].

The formation of PWs could not be understood within the framework of the extended SM. Taking into account the observed features, one may speculate that PWs might actually be chevron structures of an underlying short wavelength (thus unresolved by the optical microscope) pattern induced by the isotropic mechanism [113]; however, at present, neither direct experimental data, nor theoretical simulations are available to prove or deny this idea.

Bent-core nematics are in general good candidates for materials exhibiting ns-EC patterns. Even if they do not have explicitly smectic phase(s), cybotactic, smectic-like clusters may occur in their nematic phase [34]. In a representative BCN (CIPbis10BB), three types of ns-EC patterns have been observed: longitudinal rolls at low  $f$  and two variants of the PW pattern, PW1 and PW2, in two distinct  $f$  ranges separated by a gap in frequencies, where no pattern formation occurs (Figure 13) [36,115]. Similar behaviour was found in some other BCNs too [114]; occasionally, the frequency gap mentioned above reduced to zero [116–118]. Instead of the nearly linear  $U_c(f)$  of prewaves in calamitics, these BCNs exhibited threshold voltages diverging on both sides of the

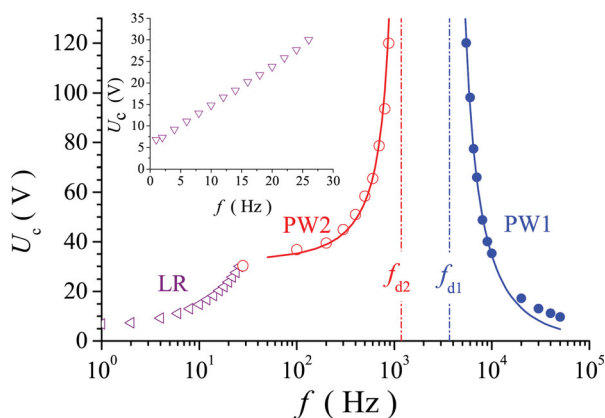


**Figure 13.** Frequency dependence of the thresholds for three pattern morphologies in the BCN CIPbis10BB ( $d = 15 \mu\text{m}$ ) [36]: ns-EC longitudinal rolls (LR) at low  $f$ , prewavy (PW2) pattern at intermediate  $f$  and prewavy (PW1) pattern at high  $f$ . The dash-dotted lines indicate the frequencies  $f_{d1}$  and  $f_{d2}$ , where  $U_c$  diverges; the solid lines are hyperbolic fit. The inset shows the LR regime on enlarged scale.

pattern-free frequency range. Unusually, pattern formation extended to much higher frequencies (up to several 100 kHz) than in calamitics; moreover, in the higher- $f$  PW range, unprecedentedly,  $\partial U_c/\partial f < 0$ , i.e., threshold voltages diminishing with increasing  $f$  were found [36, 114–118,120]. We note that the studied BCN exhibited a dielectric relaxation at an unusually low frequency ( $\sim$  kHz) [119]; as a consequence, it exhibited a double sign inversion of  $\sigma_a$  in the studied  $f$  range [36,116,118]. It is still an open question, if or how this is related to the divergence of the thresholds; nevertheless, the sign inversion frequencies do not coincide with the divergence frequencies.

In a homeotropic sample of another BCN, alignment transitions, as well as radial and tangential stripes were detected around umbilics depending on the frequency [120]. Recently, a yet unprecedented scenario, a polarity depending pattern, has been reported in a (– –) BCN [121]. At low-frequency driving, oblique rolls were detected; however, unlike regular ORs of s-EC or ns-EC that typically manifest themselves in degenerate and thus coexisting (or superposed) zig and zag domains, here the polarity of the driving voltage decided whether only zig or only zag regions are visible. It is yet unresolved, what is the cause of this symmetry breaking occurring in the wave vector selection.

### 4.3. Morphological transitions in EC

We have seen that EC may manifest itself in patterns of different morphologies. Which of them can be realized, depends on the material parameters (whether s-EC or ns-EC), on the control parameters like  $f$  (whether conductive or dielectric regime) and  $U$  (whether a pattern is at the onset or in the nonlinear regime) as well as on the alignment (planar or homeotropic) and thickness of the sample. Changing any of these parameters may induce a transition (a crossover) between morphologies. Frequency-induced transitions have already been discussed in Sections 4.1 and 4.2, transitions induced by other parameter changes are addressed below.

#### 4.3.1. Transitions induced by voltage

So far we mostly discussed the patterns emerging at the onset of the EC instability. Increasing the voltage above  $U_c$ , naturally enhances the deformation amplitude, but besides, it may alter the wave vector  $\mathbf{q}$ , the regularity, or even the morphology of the pattern.

It is a general feature of stripe patterns that upon increasing the excitation, the regular pattern becomes unstable with respect to the formation of defects (dislocations in the stripe structure, Figure 14(a)) indicating an Eckhaus instability. Unsurprisingly, this instability

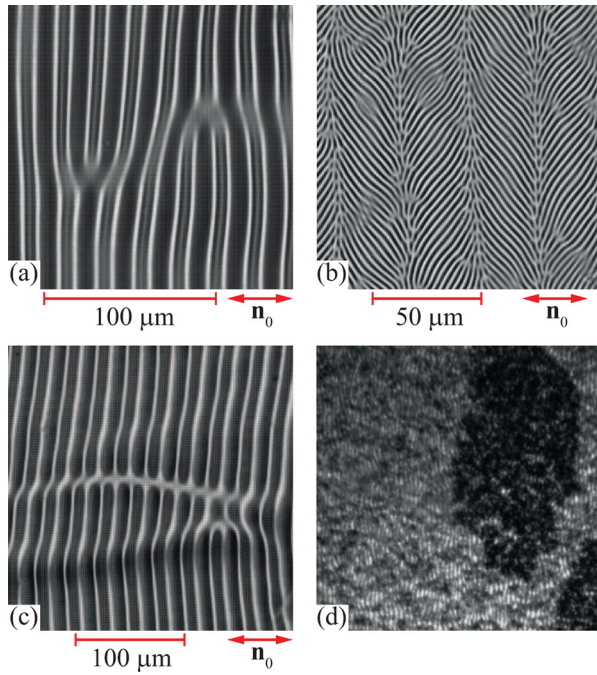


**Figure 14.** Snapshots of s-EC patterns in planar ( $- +$ ) samples well above onset: (a) defects (dislocations) in a conductive normal roll structure (Phase 5,  $d = 19 \mu\text{m}$ ), (b) dielectric (defect-mediated) chevrons (1008,  $d = 19 \mu\text{m}$ ), (c) delocalized 'long' defect in a zigzag modulated conductive normal roll structure (Phase 5,  $d = 19 \mu\text{m}$ ) and (d) coexisting domains of dynamic scattering modes DSM1 (bright) and DSM2 (dark) (MBBA, with courtesy of S. Kai, Y. Hidaka and J.-H. Huh). Shadowgraph images; the light polarization is parallel with  $\mathbf{n}_0$ .

mechanism exists in EC too. Starting with the classical example of ( $- +$ ) nematics, one finds that the behaviour is different in the two EC regimes. In the conductive regime, the Eckhaus limit is usually reached at a small  $\Delta U$  excess voltage above onset. Increasing  $\Delta U$  promotes the formation of defects in increasing numbers; the pattern becomes more and more dynamic due to defect motion and finally the sample reaches defect chaos: a state characterized by chaotic, turbulent flow and hence by strong light scattering. This state is also known as a dynamic scattering mode, which even has two variants (the weakly turbulent DSM1 and the strongly turbulent DSM2) with sharp boundaries between them [122–125]. They can be distinguished by their contrast (Figure 14(d)) and the symmetry characteristics of light scattering (it is anisotropic for DSM1 and isotropic for DSM2).

In the dielectric regime, defects appear again at fairly low  $\Delta U$ , however, the scenarios at higher voltages are different. After the number of dislocations has increased, the defects start to align in parallel chains running perpendicular to  $\mathbf{n}_0$ , forming a quasiregular superstructure, the chevrons (Figure 14(b)) [126]. The distance

between the chains is much larger than the wavelength of the dielectric rolls, which remain visible in the regions between the chains, though rotated alternately in opposite directions (the azimuthal angle switches its sign at the defect chains). This self-organization of the defects was explained theoretically [127] and confirmed experimentally [5]. We note that chevrons are not exclusive to the dielectric regime of EC. Although they do not occur in the conductive regime in planar samples, chevrons of conductive EC were reported for homeotropic ones [84].

The vicinity of the crossover frequency  $f_c$  is worth a special attention. Upon increasing  $U$ , for  $f < f_c$  the route to chaos is observed as told above for the conductive regime. If, however,  $f$  is just above  $f_c$ , the condition  $f < f_{\text{cut}}$  yet holds, i.e., conductive rolls may exist, even though their threshold is higher than the dielectric one. Experiments have proven that the conductive EC pattern is more robust; when the voltage reaches this higher, conductive  $U_c$ , the conductive EC pattern emerges and suppresses the dielectric one.

Besides the Eckhaus mechanism, there exist other destabilization mechanisms of regular s-EC patterns (see Figure 6). Another example is the *zigzag* (ZZ) instability, observable in a frequency range  $f_L < f < f_{AR}$ , which corresponds to a long wavelength undulation of the normal rolls (i.e., a voltage-induced transition towards oblique rolls, Figure 15(a)) [46,128,129]. At higher voltage, a bimodal varicose (grid-like) pattern may occur (Figure 15(b)). For  $f > f_{AR}$ , instead of the modulation of the direction of  $\mathbf{q}$  in ZZ, another instability occurs at a critical excess voltage  $\Delta U_{AR}$ . The resulting pattern, called abnormal rolls (AR), preserves the NR roll structure (i.e.,  $\mathbf{q}$ ), but causes a homogeneous azimuthal rotation of the director. The NR–AR transition corresponds to a forward pitchfork bifurcation; the azimuthal rotation angle  $\Phi$  is degenerate in its direction (left or right) and increases with the voltage as  $|\Phi| \propto \sqrt{\Delta U - \Delta U_{AR}}$  [84,130]. Abnormal rolls are present also for  $f < f_{AR}$ , pretending that the voltage is above the restabilization curve in Figure 6 [129]. The rotation of the director signals a symmetry breaking. The interpretation of the phenomenon became possible via a generalization of the weakly nonlinear theoretical description: in addition to the GLE for the amplitude (refer to Section 4.1), another GLE for the azimuthal angle  $\Phi$  had to be introduced, with cross-coupling terms in both equations [129,131,132].

The two degenerate azimuthal directions appear in domains, which extend to a size being several times the wavelength (Figure 15(c)). Under the usual observation conditions (by a shadowgraph technique or by crossed polars with one polarizer parallel to  $\mathbf{n}_0$ ), the two kinds of AR domains produce the same optical contrast; thus, only the domain boundaries may be visible.

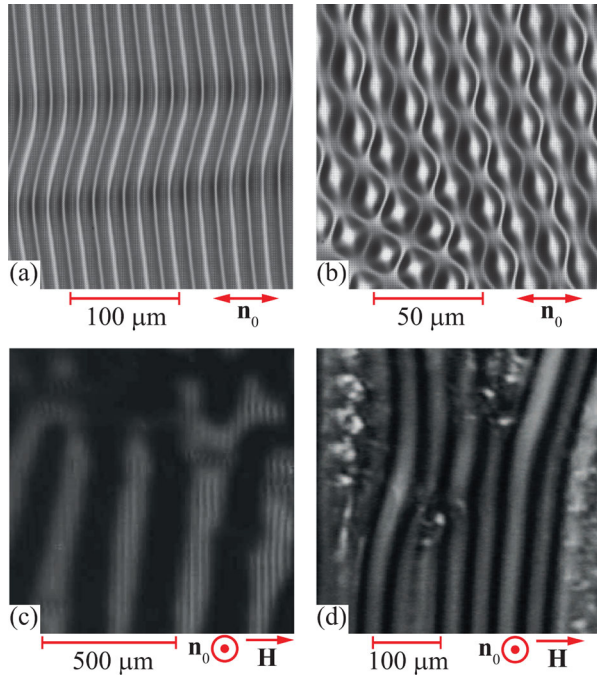


**Figure 15.** Snapshots of s-EC patterns in planar (− +) samples well above onset: (a) zigzag instability of conductive normal rolls, (b) bimodal varicose pattern in planar Phase 5 ( $d = 19 \mu\text{m}$ ); shadowgraph images, the light polarization is parallel to  $\mathbf{n}_0$ , (c) abnormal rolls (crossed polarizers, light polarization at  $8^\circ$  from  $\mathbf{H}$ ) and (d) CRAZY rolls (both polarizer and analyser are parallel with  $\mathbf{H}$ ) in homeotropic Phase 5A ( $d \approx 30 \mu\text{m}$ ).  $\odot$  and  $\leftrightarrow$  indicate out-of-plane and in-plane directions of  $\mathbf{n}_0$ , respectively, the arrow shows the direction of the magnetic field  $\mathbf{H}$ .

In order to distinguish the domains, the polarizer has to be rotated from  $\mathbf{n}_0$ . In planar samples,  $\Phi = 0$  must fulfil at the substrates; thus, due to the adiabatic light propagation, AR domains are hard to be observed; their visualization requires special techniques [61,74]. Therefore, AR domains are best seen in homeotropic samples, where the substrate makes no constraint on the azimuthal angle [84,130, 133,134]. At high voltages, a specific structure, the CRAZY roll, was also detected. This acronym, coming from ‘convection in a regular array of  $z$ – $y$  disclination loops’, expresses the essence of the structure (Figure 15(d)) [130].

An interesting crossover region is found around the frequency, where the s-EC normal rolls change to the ns-EC prewavy pattern. Here again, in a limited frequency range, increasing the voltage above the onset, the threshold of the other pattern may be reached; then the two kinds of patterns appear superposed. Recalling that in the PW pattern, the azimuthal angle  $\Phi$  of the director has a sinusoidal modulation along  $\mathbf{n}_0$  and the normal rolls should be perpendicular to the local director, it results in a chevron-like structure with oppositely curved rolls having the wavelength of the NR (Figure 12(c)). As due to

the continuous variation of  $\Phi$ , there are no defects in this structure, it is called defect-free chevron [135], in contrast to the classical dielectric chevrons, which are defect mediated.

At higher frequencies, after emerging, PW remains stable for quite large  $\Delta U$ ; then a disclination loop appears in the sample along a PW stripe. Inside the loop, the PW stripe becomes periodically modulated, i.e., wavy (which explains where the name prewavy comes from [56]) (Figure 12(b)). The wavy pattern may also superpose with NR (Figure 12(d)).

In homeotropic (+ −) nematics, the nonlinear behaviour depends strongly on the frequency. For  $f < f^*$ , where rolls appear at onset, increasing the voltage leads to defect chaos. For  $f > f^*$ , however, the *soft squares* of the onset pattern transforms into domains of a differently oriented, very regular grid pattern (*hard squares domains*, Figure 16(a)), which are separated by sharp boundaries [82,136] and coarsen with time [137]. Chaos also appears here at high voltages, however, with a discontinuous transition. In this geometry, as the azimuthal degeneracy of the orientation breaks during the pattern onset, Swift–Hohenberg equations should be used instead of the GLE [53]. Simulations provided good match with the experimental morphological phase diagrams [82,136].

In planar (+ −) nematics, the parallel rolls become zigzag modulated when moving toward higher voltages (Figure 16(b)) [82]. In 4, *n*-nonyloxybenzoic (9OBA), a well-ordered square pattern was also observed at a high voltage [138].

The patterns introduced above (apart from those involving disclination loops) are common in one feature: their amplitude (e.g., the director tilt  $n_z$  or the azimuthal angle  $\Phi$ ) increases continuously with increasing the voltage, i.e., those instabilities represent a forward bifurcation. There are conditions, however,

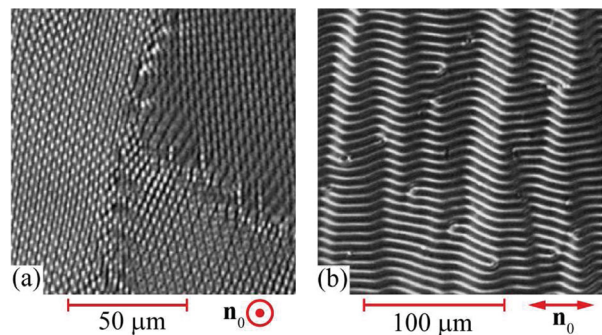


**Figure 16.** Snapshots of s-EC patterns in a (+ −) swallow-tail nematic compound well above onset: (a) hard squares in a homeotropic sample ( $d = 11 \mu\text{m}$ ), (b) zigzag modulated parallel rolls in a planar sample ( $d = 11 \mu\text{m}$ ).  $\odot$  and  $\leftrightarrow$  indicate out-of-plane and in-plane directions of  $\mathbf{n}_0$ , respectively. Shadowgraph images; the light polarization is horizontal.

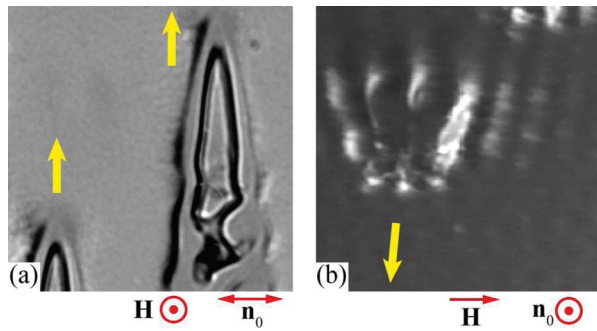


**Figure 17.** EC patterns growing into the homogeneous initial state: (a) dendrites in planar MBBA in magnetic field (by courtesy of J.T. Gleeson), (b) paw-like structure in homeotropic Phase 5A. The yellow arrows show the direction of propagation of the front.  $\odot$  and  $\leftrightarrow$  indicate out-of-plane and in-plane directions of  $\mathbf{n}_0$  or the magnetic field  $\mathbf{H}$ , respectively. Shadowgraph images; the light polarization is horizontal.

when the pattern appears at onset with a sudden jump to a finite amplitude, corresponding to a backward bifurcation [59,139]. Growth of such patterns occurs via the motion of their sharp boundaries. Backward bifurcations are always accompanied by a hysteretic behaviour; the pattern disappears at a voltage lower than its onset one. In the voltage range of the hysteresis, an intermittent behaviour may be detected.

Backward bifurcations are unfrequent in EC; they may require special combination of material parameters and/or application of additional fields. For example, it has been shown both theoretically [140] and experimentally [141–143] that in planar MBBA, a destabilizing magnetic field  $\mathbf{H}$ , being parallel to the electric field  $\mathbf{E}$ , may change the character of the bifurcation to EC: for  $H$  below a critical  $H_c$  value, the usual forward bifurcation is found, while for  $H > H_c$ , the bifurcation becomes backward and hysteresis appears. Under this latter condition, the EC pattern grows into the initial state in the form of penetrating dendrites (Figure 17(a)) [141–143]. Similar localized, travelling paw-like EC patches were reported in homeotropic Phase 5A (Figure 17(b)) [86]. Preliminary measurements on similar samples indicated accidental intermittent oscillations in the presence of an in-plane magnetic field. EC dendrites have also been observed in another geometry, in 4, *n*-octyloxybenzoic acid (8OBA) [a nematic with temperature-induced transition from (+ +) to (+ -) type] [78]. Propagation of EC fronts was also reported in a planar (+ -) sample, though the presence of a hysteresis could not be approved [82].

#### 4.3.2. Transitions induced by material parameters

The existence and/or the characteristics of patterns depend on a large number of material parameters;

therefore, it is natural to expect that changes in those parameters may alter the pattern. The recognition that some parameters are more vital than others in determining what kind of pattern may arise, initiated the classification of nematics into groups by the signs of their dielectric and conductivity anisotropies in Section 4.

While this grouping turned to be very convenient and useful, one should not forget that it is not fully precise: the transitions between different pattern types (s-EC and ns-EC) do not occur exactly at the sign inversion. For example, for (- +) nematics, if  $\sigma_a$  diminishes below a small but still positive value, s-EC ceases to exist. This was shown analytically using the 1D approximation [42] and could be confirmed by simulations using the SM. As another example, if in planar (+ +) materials  $\varepsilon_a$  is small and thus the Freedericksz threshold voltage  $U_F$  is fairly high, s-EC may occur until  $U_c < U_F$  holds [41,144]. A recent experimental proof for the latter has been reported in a twisted nematic cell [145].

Tuning the material parameters is a tedious task, involving a lot of chemistry. Unlike other parameters, electrical conductivity is a quantity, which depends more on the properties of the ionic contaminants than on the chemical structure of the nematic; therefore, the conductivity can successfully be modified by doping with conducting salts. Recently, it has been proven that a DC bias voltage also has a substantial influence on  $\sigma_{\perp}$  and  $\sigma_a/\sigma_{\perp}$  [146].

In the early times of EC research, adjustments of  $\varepsilon_a$  were attempted by mixing nematics with different dielectric anisotropies [147]; mixing, however, modifies other (elastic, viscous, etc.) parameters too. Changing the temperature has a similar disadvantage: all parameters are affected; therefore, temperature-induced variations of the onset voltages are practically unpredictable. Nevertheless, exploring the complexity of the changes of pattern morphologies and their onset characteristics has been attempted in several (calamitic and BCN) materials, as a function of temperature, voltage and frequency [39,97,148,149]. Temperature-induced transitions between pattern morphologies were detected in compounds exhibiting a sign inversion of either  $\sigma_a$  [97,110] or  $\varepsilon_a$  [150] in the nematic phase.

All nematics mentioned so far are uniaxial materials. EC measurements were also performed using a BCN material, which was claimed to exhibit a temperature-induced uniaxial nematic to biaxial nematic phase transition [151]. A morphological transition (actually a divergence of a pattern threshold) was detected at the transition temperature, which was attributed to conductivity variation.

A sign inversion of  $\sigma_a$  or  $\varepsilon_a$  may occur even at a fixed temperature, if the compound has a dielectric relaxation.

Typically, dielectric dispersion in calamitic nematics occurs at very high ( $\sim$  MHz or above) frequencies, where no pattern formation is reported. Occasionally, however, the relaxation frequency may fall into the range relevant for EC. One such example is a nematic capable of dual frequency addressing, where  $\varepsilon_a$  changes sign in the audio frequency range. There, a crossover between the Freedericksz and the electroconvecting states can be induced by changing  $f$  [152]. Recently, the influence of the driving waveforms on the threshold of the patterned states has thoroughly been analysed using such a compound [153]. As another example, some bent-core nematics exhibit a low  $f$  dielectric dispersion and as a result, they show a double sign inversion of  $\sigma_a$ , as already mentioned in Section 4.2.

Material and/or cell parameters can also be modified by doping the nematic with nanoparticles. In a recent experiment, a nematic doped with gold nanoparticles exhibited reversed electro-optical switching compared to that of the undoped material [154]. The phenomenon was attributed to a change of orientation from planar to homeotropic due to doping on the one hand, and to the appearance of EC rolls characteristic for  $(+ -)$  nematics, not present in the undoped material, on the other hand. Unfortunately, the sign of  $\sigma_a$  has not yet been measured; thus it is yet unclear, if  $\sigma_a < 0$  holds and if so whether that is also the consequence of doping.

While adjusting material parameters is difficult in experiment, it is much simpler in theory. Checking the influence of material parameters on  $U_c(f)$  and  $q_c(f)$  of s-EC can easily be done by numerical simulations based on the (extended) SM, by modifying one parameter, while keeping the others unaltered. For example, it has been known for a long time that the enhancement of  $\sigma_{\perp}$  reduces  $U_c$  and  $q_c$  in the conductive regime, while increases them in the dielectric one; as a result, the crossover frequency  $f_c$  shifts to higher values. Recently, it has been proven that the enhancement of the relative conductivity anisotropy  $\sigma_a/\sigma_{\perp}$  diminishes  $U_c$  and  $q_c$  in both regimes, but increases  $f_c$  [146].

Unfortunately, similar parameter tests are missing yet for ns-EC.

Exploring the influence of certain material parameters on pattern behaviour is also important to find a strategy to avoid pattern formation. Simulations provide useful hints for the proper adjustment of parameters in order to reach that goal.

## 5. Pattern formation at ultra-low frequencies (flashing)

The patterns discussed so far were observable either at DC excitation or at AC with such frequencies where the

longest characteristic time of the system, the  $\tau_d$  director relaxation time, is much longer than the period  $T = f^{-1}$  of the excitation. If the driving frequency is reduced to the subhertz range, this assumption fails; nevertheless, pattern formation occurs even at such (ultra)low  $f$ . There  $T/2 < \tau_d$  holds; as a consequence, dynamics of the system changes and new phenomena can be observed. Namely, the director has enough time to build up a spatial distortion and then decay back to the basic state, still within a half period of the sinusoidal driving voltage; thus the pattern amplitude is changing all the time. This scenario is expected to occur during Freedericksz transitions and the formation of FDs or EC as well.

Intuitively, one would expect a smoothly growing and then diminishing pattern contrast, roughly following the evolution of the voltage. Instead, the extended SM [which is valid also in this ultra-low  $f$  range, for FDs as well as for EC] concluded that director distortion (and thus the pattern) should exist only in certain short portions of the driving period [27]. For visual observations, this would mean repetitive flashes (short pulses) of the pattern. Experimental studies (which are rather scarce [32,58,60,65]) confirmed this behaviour, as will be shown below.

The transition from the audio frequency conductive s-EC with quasi-stationary director configuration to the low  $f$  flashing regime was experimentally explored in Phase 5, using controllable (high) speed imaging [60,65]. For quantifying the recorded image sequences, the contrast  $C_s$  was defined as the mean square deviation of the image intensity. In order to compare the behaviour at different frequencies, Figure 18(a) depicts the normalized contrast for a single period ( $T$ ) of the driving voltage at various frequencies.

At  $f = 100$  Hz, the contrast is almost constant, as it was expected; the small second-order  $2f$  modulation is just perceptible. At one decade lower  $f$ , the contrast modulation becomes larger, but the pattern is still visible in the entire period; however, at  $f = 1$  Hz, as a qualitatively different behaviour, the pattern is not always visible (the contrast reached the background value). At even lower frequency ( $f = 100$  mHz), EC appears only in narrow time windows as short flashes, in each half period. The apparent symmetry breaking observed as the inequality of peak heights in the positive and negative half periods was attributed to perturbation by a small offset voltage, confirmed by the theory. The frequency dependence of the relative contrast modulation clearly showed the transition from the stationary to the flashing character with a transition frequency well approximating  $\tau_d^{-1}$ . For comparison, Figure 18(b) shows the temporal evolution of the director component  $n_z$  in the midplane of the sample within one period, calculated by the extended SM

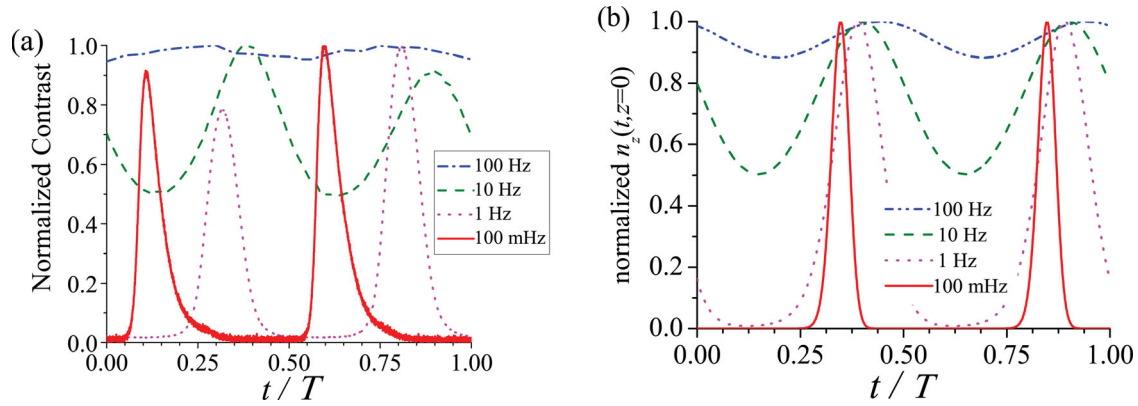


**Figure 18.** The time dependence of (a) the measured normalized contrast and (b) the calculated director component  $n_z$  in the midplane of the sample, within one voltage period ( $T$ ) at different driving frequencies for conductive EC in the compound Phase 5 [60].

for conductive EC at the same frequencies. Though the relation of the contrast to  $n_z$  is nonlinear, the qualitative agreement with the experiments is evident. At higher  $f$ , the time instants of the maximal contrast and  $n_z$  within the period even match quantitatively, however, a significant difference in their phase is seen at low  $f$  [60].

At low  $f$ , deviation was also found between the measured and calculated threshold voltages. Both discrepancies could be minimized by taking into account the internal structure of the test cell: insulating orienting layers between the electrodes and the liquid crystal result in an internal voltage attenuation and phase shift at low  $f$ . By fitting  $f$ -dependent electric current measurements with parameters of an equivalent circuit model, correction of the experimental data could be done [60], considerably reducing the mismatch compared to the theory. The remaining difference was attributed to the stronger effect of non-ohmic ionic conductivity at lower frequencies, which is not taken into account by the theoretical description.

Besides the flashing character, an interesting feature of the pattern formation at ultra-low frequencies is that the intersection of the  $U_c(f)$  threshold curves of flexodomains and EC, i.e., a crossover between FDs and EC, may occur in this frequency range [32,60]. The behaviour of the threshold curves of FDs and EC is illustrated in Figure 19(b) for another calamitic compound 4-*n*-octyloxy-phenyl 4-*n*-methoxybenzoate (10O8). At higher  $f$ , the EC threshold is sharp, but for  $f < 1$  Hz, the contrast versus voltage curve becomes gradually smoother. The lack of sharp threshold at low  $f$  was attributed to the effect of the nonlinear current characteristics (see Figure 19(a)), which might exhibit spatial dependence due to small variations in the boundary conditions. The lowering of the EC threshold on decreasing frequency for  $0.5 \text{ Hz} < f < 10 \text{ Hz}$  is in accordance with previous theoretical and experimental findings in other liquid crystals [155]. The increasing tendency of the EC threshold at ultra-low  $f$  may partially be attributed to the internal voltage attenuation originating from the

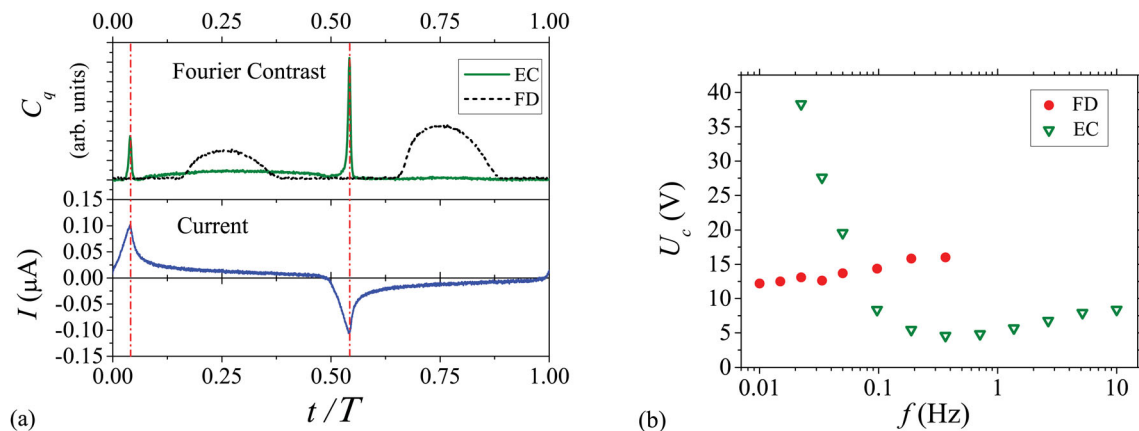


**Figure 19.** The time dependence within a sinusoidal driving period  $T$  (a) of the Fourier contrast  $C_q$  and the electrical current  $\bar{i}$  flowing through the liquid crystal 10O8.  $t = 0$  corresponds to the zero crossing (from positive to negative) of the applied sinusoidal voltage. (b) The threshold voltage of EC and flexodomains (FD) determined from various methods as a function of frequency on 10O8 [32].

insulating polyimide layers, and the screening of the ionic double layers close to the substrates. For FDs, the variation of the threshold voltage was found to be weaker than for EC in the low  $f$  regime. Considering that the internal voltage attenuation is larger at lower  $f$ , the actual threshold voltage would decrease at  $f \rightarrow 0$ , similarly to previous theoretical findings [27].

A speciality of the crossover of flashing FDs and EC at ultra-low  $f$  is that both kinds of patterns appear in the whole sample, just in different time windows [32,60], unlike at the crossover of EC patterns at high frequencies, where the coexistence of the two patterns means either their superposed or spatially separated appearance. It means that if the applied voltage is higher than both threshold voltages, EC and FDs appear as time separated, alternating flashes. This time separation of patterns allows to determine the threshold voltages of both patterns in an extended frequency range on both sides of the FD–EC crossover frequency (see Figure 19(b)). If the voltage is between the two thresholds, only flashes of the pattern belonging to the lower threshold occur. This scenario applies for a relatively wide frequency range on both sides of the crossover frequency, even when the two pattern thresholds are significantly different. For  $f \gtrsim 0.4$  Hz, the time separation of the two kinds of patterns ceases; the two contrast peaks merge into one. Finally, at even larger  $f$ , FDs do not appear; only EC remains detectable.

The recognized importance of ionic phenomena in liquid crystals during the pattern formation at ultra-low  $f$  motivated further investigations with synchronized electrical current measurements [32] in the rod-like compound 4-*n*-octyloxy-phenyl 4-*n*-methyloxybenzoate (10O8) that showed alternating flashes of oblique EC and FDs in a wider  $f$  range compared to Phase 5. The two kinds of patterns are separated not only in time, but also in the Fourier space. This behaviour is demonstrated in the upper panel of Figure 19(a), showing the temporal evolution of the contrast  $C_q$  of each pattern. Here,  $C_q$  is defined as the sum of the spectral intensities within a region around the characteristic Fourier peak of the given pattern. It is seen that the EC flash (solid line) closely follows the time reversal of the applied voltage, while FDs (dashed line) are present rather around the voltage maxima/minima.

The temporal evolution of electric current  $\tilde{I}$  flowing through the cell is plotted in the lower panel of Figure 19(a). It clearly displays a non-ohmic character. The current peaks after each polarity change of the applied voltage coincide precisely with the flashes of EC [32]. For different frequencies, voltages and temperatures, the peaks in  $\tilde{I}$  and the EC flashes were found to occur at the same time instants. The current peaks are

also present at voltages below the EC threshold, and in the isotropic phase as well, thus they do not originate from the pattern formation. Rather, the current peak seems to trigger the EC so that it occurs earlier than is expected from the SM, explaining the phase difference between theory and experiment at  $f = 100$  mHz in Figure 18.

The nonlinear current response is attributed to the ionic conductivity of the material and the insulating orienting layers on the electrode surfaces (blocking electrodes). The ionic conductivity arises due to the low concentration of ions that are accelerated by the applied electric field. If the field changes slowly, the charge carriers have time to accumulate at the boundaries forming double layers, because charge injection is hindered by the insulating coatings. After the polarity reversal, the forces acting on the charges turn to the opposite direction causing a large ionic flow, since the previously formed double layers have to be destroyed and built up on the opposite electrodes. This mechanism does not depend on the anisotropy of LCs. Indeed, previous theoretical studies [156,157] yielded nonlinear current response to low  $f$  sine voltage driving, similar to the  $\tilde{I}(t)$  in Figure 19(a). In order to explore the influence of the anisotropy of LCs, the weak electrolyte model [55] should be used instead of the SM; however, the WEM has not yet been analysed in the relevant low- $f$  regime.

Dielectric s-EC has a different temporal dynamics compared to conductive EC:  $n_z$  oscillates with the driving voltage even at high frequencies. This behaviour, namely that the polarity of  $n_z$  is alternating in subsequent half periods, naturally persists also for ultra-low  $f$ . The transition from the high  $f$  to the low  $f$  regime means that  $n_z = 0$  occurs not only for a time instant, but for a gradually increasing interval in each half period of driving. This was shown experimentally using the mixture Phase 4, which had exclusively dielectric EC in the whole  $f$  range, due to its fairly low electrical conductivity [58]. The crossover between FDs and dielectric EC in the form of alternating flashes was also observed.

We note that, while the conductive and dielectric regimes are clearly distinguishable at high  $f$  via the temporal dynamics of  $n_z$  (stationary versus oscillating) as well as by the wavelength of the patterns, it is not so easy at ultra-low frequencies by two reasons. On the one hand, in the flashing regime,  $|n_z(t)|$  of the conductive and the dielectric EC are almost identical, but  $n_z$  changes sign from one half period to the other in the dielectric flash, while in the conductive flash it does not change sign. Under the usual observation conditions, optics is not sensitive to the sign of  $n_z$ , therefore observation of the time evolution of the patterns does not allow distinguishing. On the other hand, at ultra-low  $f$ , the wavelengths of the two kinds of patterns are less diverse.

In the audio frequency range, switching from sinusoidal to square wave (SQW) driving makes only minor quantitative differences in the pattern forming behaviour; the ultra-low  $f$  driving is, however, more sensitive to the waveform. Namely, at SQW applied voltages, the scenarios presented above and illustrated in Figure 19(a) (the alternating EC and FD flashes) do not exist. Instead, a transient pattern occurs immediately after the polarity reversal (presumably oblique rolls of s-EC induced by an ionic current peak) which, after about a second, relaxes to a steady state corresponding to the amplitude of the SQW voltage. Seemingly, there is a switching between two DC states of opposite polarity. This steady state may be the initial homogeneous one or a DC patterned state (FD or EC, depending on the material parameter set). Relaxation to the homogeneous state indicates that the threshold voltage for the onset of the transient is lower than the threshold for any DC patterned state.

Pattern formation was also studied in  $90^\circ$  twisted planar cells using ultra-low-frequency SQW voltage excitation, in a rod-like [145] as well as in a bent-core compound [40]. In the rod-like compound, transient roll structures appeared immediately after the polarity reversal of the voltage that decayed in a few seconds. The direction of  $\mathbf{q}$  was polarity dependent; it indicated that the maximum director distortion is located in the vicinity of the negative electrode, instead of being in the middle of the cell. The bent-core compound showed flexodomains with similar polarity-dependent behaviour [40] at low frequencies. Using DC voltage, the static patterns appeared in domains of different stripe directions separated by disclination lines. However, with low  $f$  AC excitation at low voltages, the transient alternation of  $90^\circ$  rotated stripes was observed yielding that the director deformation was localized near the surfaces. A similar effect – flexodomains with their direction parallel to the rubbing direction of one or the other substrate depending on the polarity of the voltage – was found also in a  $18^\circ$  twisted cell using another BCN [158]. The effects seen in both the rod-like and the bent-core material were interpreted as the consequence of the ionic effect in the liquid crystal leading to strong transient electric field gradients near the electrodes, where the flexoelectric polarization can assist the emergence of convective patterns of the Carr–Helfrich mechanism and also the formation of FDs.

We remind here (cf. Section 4.2) that a polarity-dependent  $\mathbf{q}$  has been found in another bent-core nematic, however, in a planar (no twist) geometry [121], where the above interpretation is not applicable. It is yet unclear, which material parameters or boundary conditions decide, whether surface induced or bulk flexodomains and whether polarity-dependent or

polarity-independent patterns become observable in a given material.

## 6. Driving with other, non-sinusoidal waveforms

The patterns reported so far were excited mostly by AC voltage of sinusoidal waveform. Using square wave (SQW) signals is another option. In the audio frequency range, switching from sinusoidal to square wave does not change the scenarios qualitatively. This is not, however, the case at ultra-low frequencies, in the flashing range (cf. Section 5).

In recent decades, patterns induced by more complex waveforms have also attracted attention; superposition of an AC voltage with another AC or DC voltage, as well as the case of stochastic driving will be addressed in Sections 6.1, 6.2 and 6.3, respectively, in more detail.

### 6.1. AC+AC driving

The problem of pattern formation under superposing two AC voltages of different frequencies ( $f_l < f_h$ ) and rms values,  $U = U_l \sqrt{2} \sin(2\pi f_l t) + U_h \sqrt{2} \sin(2\pi f_h t)$ , becomes especially interesting, if the two frequencies belong to different EC regimes; i.e., if the relation  $f_l < f_c < f_h$  fulfils. Then the patterns induced by a single component, conductive EC for  $f_l$  and dielectric EC for  $f_h$ , have different temporal dynamics; therefore, the result of a mixed driving is nontrivial. The main question is to find the stability limiting curve (SLC) in the  $U_h$ – $U_l$  plane, i.e., the border of that region where the applied ( $U_h, U_l$ ) voltage combination is not sufficient to induce pattern.

In a pioneering work [159], two AC voltages (actually SQW signals) of commensurate frequencies,  $f_h = 4f_l$ , were superposed in phase and the resulting pattern formation was investigated experimentally in Mischung 5, as well as theoretically by a Floquet analysis. The SLC obtained was composed of three branches. Starting at  $U_h = 0, U_l \neq 0$ , there is a branch with conductive normal rolls with increasing  $U_l$  threshold upon adding  $U_h$ . Another branch originates from  $U_h \neq 0, U_l = 0$ , corresponding to dielectric rolls, where the  $U_h$  threshold decreases upon adding  $U_l$ . Finally, along the third connecting branch, at intermediate  $U_h, U_l$  values, a subharmonic pattern with a repetition frequency of  $f_l/2$  was observed (Figure 20). The transitions between these pattern morphologies are sharp, characterized by jumps in the wave number of the pattern. Similar results were obtained also in [160]. A good match between observations and theoretical predictions was found. The shape of the SLC remained qualitatively unaltered when changing the frequency, pretending that the conditions  $f_l < f_c <$

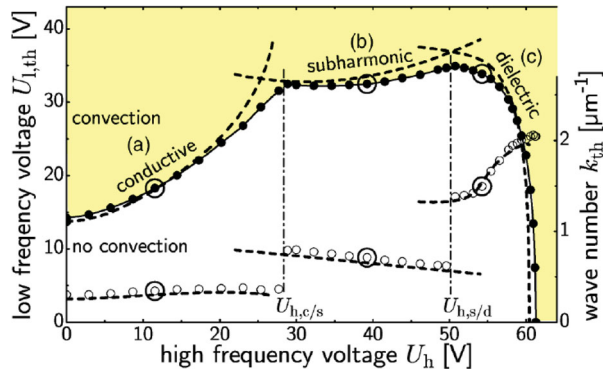


**Figure 20.** Measured threshold voltages for the pattern onset ( $\bullet$ ) and selected wave numbers ( $\circ$ ) for in-phase superposition of  $f_l = 80$  Hz and  $f_h = 320$  Hz square waves. The convection-free ground state is surrounded by a conductive (a), a subharmonic (b) and a dielectric regime (c). The selected wave numbers jump at the transitions between these regimes. Circles mark the parameters ( $U_l, U_h$ ) where the images of Figure 2 of [159] have been taken. Dashed lines show calculated thresholds and wave numbers extracted from the (global) minimum of the neutral curve  $N$  in the  $U_l$ - $k_x$  plane for given  $U_h$  (cf. Figure 7 of [159]). Reprinted figure with permission from [159]. Copyright (2004) by the American Physical Society.

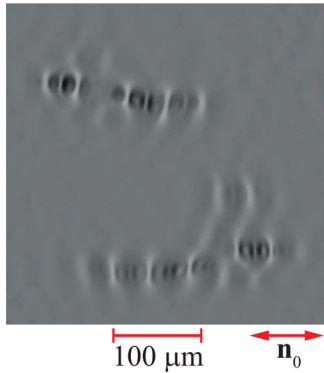


**Figure 21.** Worms detected in 1008 at superposing two AC voltages of different frequencies ( $d = 50$   $\mu\text{m}$ ) [146].  $\leftrightarrow$  indicates the in-plane directions of  $\mathbf{n}_0$ . Shadowgraph image; the light polarization is parallel with  $\mathbf{n}_0$ .

$f_h = 4f_l$  were met [161]. A slight deviation was found only at low  $f_l$ , where the  $U_l(U_h)$  curve of the dielectric branch of the SLC exhibited a non-monotonic behaviour. As a result, in a narrow  $U_h$  voltage range, reentrance of pattern formation, namely a dielectric EC-homogeneous state-dielectric EC transition, was detected upon increasing  $U_l$  [161].

It was also shown that subharmonic patterns may still exist, even if the phase shift between the commensurate frequencies is nonzero; however, if the phase shift becomes larger than about  $40^\circ$ , subharmonic patterns cannot be exited any more. Then only the conductive and the dielectric branches remain in the SLC, with a

direct transition between these morphologies [162,163]. Obviously, no subharmonic pattern is expected if  $f_l$  and  $f_h$  are incommensurate, because the superposed driving signal is not periodic. Indeed, recent measurements reported localized, worm-like EC structures instead of subharmonic pattern at the connecting branch of the SLC [146]. Similar worm structures have previously been reported under pure sinusoidal driving in the conductive NR regime of MBBA and Phase 5 [164], as well as in the conductive OR regime of I52 [139]. The latter was interpreted within the amplitude formalism, via the coupling of four  $\mathbf{q}$ -modes [139,165–167].

We note that superposition of two specific AC voltages is not a necessary condition for observing subharmonic EC patterns. It was shown that excitation with time-asymmetric (e.g., sawtooth-like) waveforms may also do this job [168]. If the measure of the time asymmetry is large enough, the subharmonic pattern may appear in a frequency range between the conductive and dielectric regimes. Then, instead of the usual transition sequence shown in Section 4.1.1, a conductive EC-subharmonic EC-dielectric EC sequence can be detected, where each transition is accompanied with the jump of the wave number [168].

Superposition of two AC voltages of commensurate frequencies provides an opportunity to study the influence of time reversal on the pattern formation. Carefully choosing the phase of the two voltages depending on the  $f_l:f_h$  frequency ratio, time-mirrored pairs of waveforms can be selected. Theoretical calculations based on the SM have concluded that the time reversal should have no influence of the SLC [163]. Indeed, experiments with superposing SQW signals of 1:4 frequency ratio seemed to justify this conclusion. Later tests with sinusoidal waveforms and various (1:2, 1:3 and 1:4) frequency ratios have, however, shown that under certain conditions (e.g., when  $f_l$  is close to  $f_c$ ) time reversal causes a detectable deviation in the thresholds, i.e., the two SLC curves do not coincide [169].

Finally, we note that simulations have been extended to nonstandard EC too. They concluded that upon changing the sign of  $\sigma_a$ , not only the conductive regime disappears [54,160], but a subharmonic solution also becomes unrealizable [160].

## 6.2. AC + DC driving

The aim of studying patterns driven by superposed AC and DC voltages,  $U = U_{dc} + U_{ac}\sqrt{2}\sin(2\pi ft)$ , is similar to that described in the previous Section 6.1: to find the boundaries of the voltage region, in which the initial homogeneous state remains stable despite applying a combination ( $U_{ac}, U_{dc}$ ); moreover, to explore the

morphologies of the pattern emerging at crossing this stability limit. DC-driven EC patterns represent a solution of the SM with a time symmetry different from that in the conductive and dielectric regimes: all relevant variables are stationary. Due to this symmetry difference, there is no smooth transition from the AC  $f \rightarrow 0$  case to DC [27]; even if the DC threshold voltage and the critical wave number do not differ much from the AC values in the  $f \rightarrow 0$  limit.

Working with DC voltage provides extra difficulties. Neglecting ionic effects (which is a basic assumption of the SM) is the least established at DC driving. The internal voltage attenuation, which originates in the interplay of the polyimide alignment layer covering the electrodes with the finite conductivity of LCs, becomes most important at DC driving. Therefore, the voltage sensed by the LC layer is smaller than the actually measured applied voltage. This attenuation is difficult to determine; moreover, it varies among cells. Long-term application of DC voltage may adversely affect the chemical stability of the nematic, which may have consequences on reproducibility; but even in a short term, DC voltage affects the conductivity of the LC [100,146,170]. DC voltage jumps initiate relaxation processes in the conductivity, with  $\sigma(t)$  having multiple characteristic times from seconds to hours [146]. Therefore, a sample practically does not reach its equilibrium state after a DC voltage has ever been applied; the results may depend on the measurement protocol and on the history of the sample. Owing to these effects, theoretical predictions are expected to match experimental data less, compared to the case of AC driving.

On the other hand, combined (AC + DC) driving offers more possibilities in testing morphological transitions in  $(- +)$  nematics, since not only EC patterns can be induced by DC, but flexodomains also (depending

on the material parameters). In addition, AC-driven s-EC patterns can be either conductive or dielectric; thus one can investigate the interaction of patterns in four different scenarios. Theoretical predictions [146,171] could be obtained for the complete SLC for each scenario from the extended SM, by numerical calculations using various sets of material parameters. Modification of the parameters did not change the qualitative behaviour (the shape of the SLC).

For each scenario, calculations yielded a simple connected pattern-free, homogeneous region. In one case, namely when DC electroconvection interacts with a low  $f$  conductive EC, the characteristics of the pure DC- and pure AC-driven patterns are very close to each other; as a result the SLC was found to be a quarter-ellipse-like, convex curve shown as a solid line in Figure 22(a), along which the wave number and the obliqueness angle of the pattern change continuously. So, in this case, there is a smooth transition between the two types of pattern; increasing  $U_{dc}$  from zero reduces the AC threshold and vice versa, adding  $U_{ac}$  to  $U_{dc}$  reduces the DC threshold. For the remaining three scenarios, i.e., when flexodomains and/or dielectric EC is involved, the behaviour is different. Under these conditions, the pure DC and the pure AC pattern are so much different (in mechanism and/or temporal dynamics and  $\mathbf{q}$ ) that no smooth transition is possible. The SLC breaks into two branches: the DC branch starting at  $U_{ac} = 0, U_{dc} \neq 0$  (the dash-dotted line in Figure 22(a) and the solid and dash-dotted lines in Figure 23(a)) and the AC branch originating at  $U_{dc} = 0, U_{ac} \neq 0$  (the dotted line in Figure 22(a) and the dashed and dotted lines in Figure 23(a)). The two branches do not join smoothly; the point where they connect indicates a crossover of patterns, i.e., a morphological transition accompanied by a jump in  $\mathbf{q}$ . It was found that the DC branch is concave (adding an AC voltage increases the

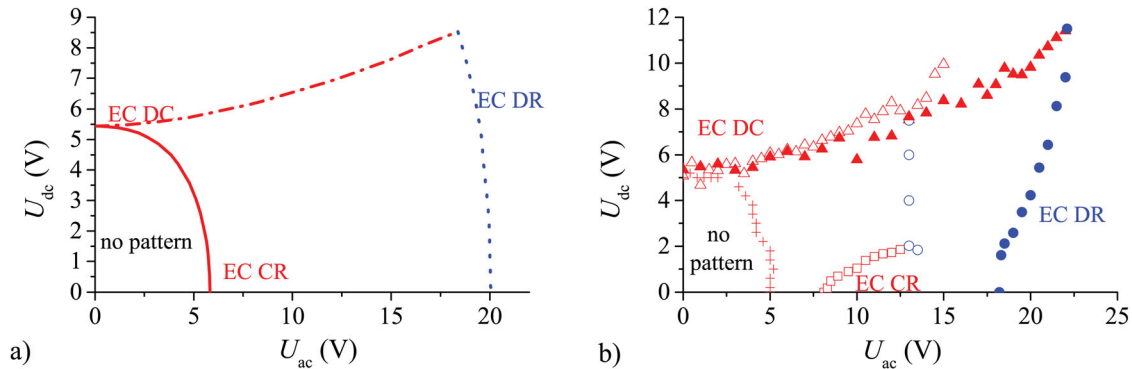


**Figure 22.** Stability diagram in the  $U_{ac}$ - $U_{dc}$  plane at two frequencies. (a) Stability limiting curve calculated with material parameters of Phase 5 for low (solid and dashed lines) and high (dash-dotted and dotted lines) frequencies. Data taken from [171]. (b) SLC measured in Phase 5 at  $f = 10$  Hz (crosses), at  $f = 80$  Hz (open symbols) and at  $f = 400$  Hz (solid symbols). EC DC, EC CR and EC DR denote DC electroconvection, conductive EC and dielectric EC, respectively. Data taken from [170].

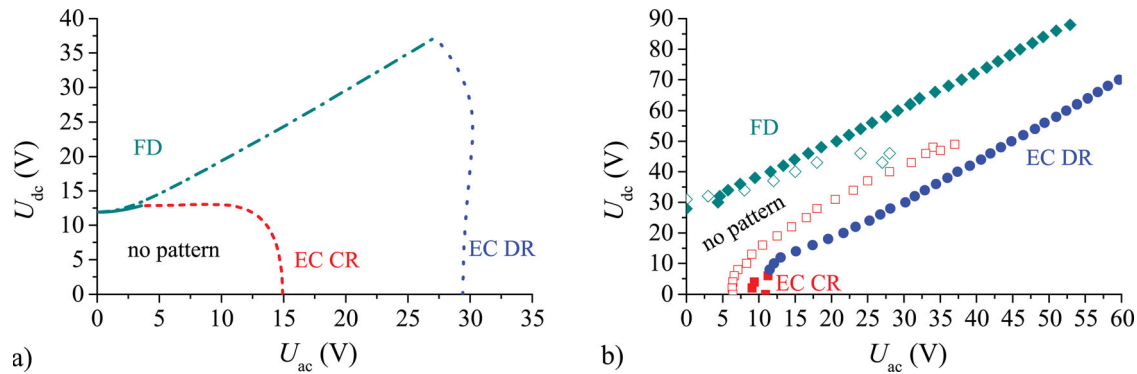


**Figure 23.** Stability diagram in the  $U_{ac}$ - $U_{dc}$  plane at two frequencies. (a) Stability limiting curve calculated with hypothetical material parameters of 1008 for low (solid and dashed lines) and high (dash-dotted and dotted lines) frequencies. Data taken from [146]. (b) SLC measured in 1008 at  $f = 2$  Hz (open symbols) and at  $f = 10$  Hz (solid symbols). FD, EC CR and EC DR denote flexodomains, conductive EC and dielectric EC, respectively. Data taken from [146].

DC threshold), while the AC branch is convex (adding a DC voltage reduces the AC threshold).

These numerical results were confirmed by approximate analytical calculations via a perturbational analysis, performed in the vicinity of the  $U_{ac} = 0$  or  $U_{dc} = 0$  points (at the origin of the DC and AC branches of the SLC) [171].

Experimental realization and exploration of the different scenarios of the pattern formation under combined driving were performed using two nematics: Phase 5 exhibited EC [170–172], while 1008 had flexodomains at DC [146]; at AC driving, EC was present in both materials. The stability limiting curves were determined at various frequencies (in the conductive as well as in the dielectric regimes). Comparison of experimental data with theoretical predictions yielded mingled results.

When DC EC was combined with conductive EC, the predicted convex SLC was reproduced (see the crosses in Figure 22(b)), however, only at the lowest test frequency [171]. Increasing  $f$ , but still remaining in the conductive regime, an extension of the stable range was observed; unexpectedly, the AC branch of the SLC became concave: superposing DC increased the AC threshold. Moreover, the AC branch broke into two segments: conductive EC (open squares) was present at low  $U_{dc}$ , but dielectric EC (open circles) occurred at higher  $U_{dc}$ . As a consequence, instead of the predicted smooth transformation, two morphological transitions were found. This behaviour indicates that the DC voltage induced a reduction of the crossover frequency  $f_c$ , which was confirmed by independent measurements too. The extension of the stable region becomes even more pronounced at frequencies, where the pure AC-driven pattern is dielectric EC. Here, both along the DC (solid triangles) and along the AC (solid circles) branch the thresholds increase upon superposing voltage of the other type (see Figure 22(b)); the

former agrees, but the latter is in contrast to the predictions of the theory. At high frequency, the AC and the DC branch run nearly parallel at high voltages, flanking a pattern-free channel. As a result, there are  $U_{ac}$ ,  $U_{dc}$  combinations where no pattern appears, even though the voltages exceed several times the pure DC and AC thresholds. As an extreme, the two branches do not even connect within the accessible voltage range (limited by the used high-voltage amplifier) [170].

The conclusion is that a signal with properly adjusted asymmetry leads to unusual, reentrant morphological sequences (EC–pattern-free–EC) when voltage is scanned either horizontally or vertically in the  $U_{ac}$ - $U_{dc}$  plane. Moreover, the asymmetrical signal suppresses undesirable turbulence and inhibits pattern formation completely. Thus, if for any reason, it is necessary to apply a high AC (DC) voltage (which is much above the pattern onset) to the cell, it is enough to superpose some DC (AC) voltage, in order to keep the system in the pattern-free channel and hence to avoid patterns.

When flexodomains existing at DC are combined with EC, the DC branch is expected to be concave (see Figure 23(a)). This feature has been proven experimentally (see the diamonds in Figure 23(b)) by several groups on different nematics [38,146,173]. For the AC branch of the SLC (squares and circles in Figure 23(b)), however, the same discrepancy was found as in the above paragraph: the curve is unexpectedly concave and the pattern-free channel may extend to high voltages, seemingly without closure [146].

In a limited frequency range, a special scenario has also been observed: the nearly parallel DC and AC branches of the SLC were connected by a third branch, corresponding also to flexodomains, however, with much shorter wavelength than FDs along the DC branch [146]. These short wavelength flexodomains seem to be the

manifestation of FDs of dielectric type, whose threshold is normally too high to be detected. The biasing by DC voltage helps to reduce this threshold, as confirmed qualitatively by numerical calculations [146].

From the studies described above one can conclude that, though some features (the behaviour of the DC branch of the SLC) nicely match with the expectations, serious discrepancies (the behaviour of the AC branch of the SLC) were also detected. Looking for the possible reasons of this discrepancy, it is reasonable to expect that due to the presence of a DC voltage one or more material parameters actually vary ( $\sigma$  is a trivial candidate), while all calculations within the SM were done assuming that material parameters are constant. The ionic effects (already mentioned at the beginning of Section 6.2) may play an important role; thus, the weak electrolyte model extended with flexoelectricity might provide a more precise description. Nevertheless, at present, such an analysis seems to be a too big challenge.

It has recently been proven that even remaining within the framework of the extended SM, a qualitative explanation can be given for the discrepancies. Impedance measurements performed simultaneously to pattern observations have indicated that the impedance of the sample (which is composed of a parallel resistance and capacitance) depends on the DC bias voltage: increasing  $U_{dc}$  the parallel resistance becomes higher [170]. Independent measurements have approved that not only the conductivity  $\sigma_{\perp}$ , but the relative conductivity anisotropy  $\sigma_a/\sigma_{\perp}$  too, diminishes upon increasing  $U_{dc}$ . Both parameters affect the threshold characteristics, as mentioned in Section 4.3.2. Thus, comparing experiments with the theoretical predictions, one should not use the SLC calculated for a fixed  $\sigma_a$  and  $\sigma_{\perp}$ , instead theoretical data should be taken from a set of SLCs, each calculated with different, experimentally obtained conductivity data belonging to a given  $U_{dc}$ . That procedure can, qualitatively, explain why pattern formation is suppressed by the superposition of DC and AC voltages [146].

The combined driving has been used from another aspect at a frequency, where an NR-ZZ-AR-varicose transition sequence occurs at increasing  $U$  [174]. In some voltage range, oscillating zigzag structures can be observed, which were decomposed into three modes: the zig, the zag and a twist mode; the latter corresponds to a homogeneous rotation of the director, like in case of AR. It was shown that the phases of these three modes become synchronized to the driving voltage if a DC voltage is superposed; such synchronisation is absent in case of pure AC driving.

For the other variant of s-EC, the (+ -) nematics, so far neither theoretical analysis, nor experimental studies

are known about the influence of superposing AC and DC voltages.

Nonstandard electroconvection under combined driving is also a mostly unexplored field yet. Though for (- -) nematics the mechanism of the pattern formation is known (originating in flexoelectricity), up to now no theoretical predictions are available. Experimentally, the limited assortment of (- -) compounds makes a constraint. Moreover, as the temporal dynamics of the longitudinal rolls of this kind of ns-EC resemble the dielectric regime of s-EC, the EC pattern may not exist at DC driving. Therefore, in some compounds, pure  $U_{dc}$  does not influence the stability of the planar state; then the SLC has only the AC branch left. Preliminary results on a representative compound, 8/7, indicate increasing AC threshold upon biasing with  $U_{dc}$  [175]. Other compounds may exhibit flexodomains at DC. As FDs and longitudinal rolls are both (nearly) parallel to the initial director and their wavelength scales roughly with the thickness, a smooth transformation between these two pattern types may be anticipated. Indeed, preliminary results on the BCN ClPbis10BB seem to confirm this anticipation [175].

For (+ +) nematics, the lack of the full understanding of the pattern formation mechanism is a big drawback. The morphological phase diagram in the  $U_{ac}-U_{dc}$  plane has yet partially been explored for planar 5CB [100]. The first instability in this compound is the splay Freedericksz transition; its SLC is a quarter circle. EC sets in as a secondary instability in the quasihomotropic state in the form of a stationary cellular pattern, both at pure AC and pure DC driving as well as at combined driving; its SLC is quarter-ellipse-like. At high  $U_{ac}$ , normal rolls were observed (independently of  $U_{dc}$ ), while at certain  $U_{ac}$ ,  $U_{dc}$  combination, a new pattern morphology, *parallel stripes*, was detected. Thus when mapping the  $U_{ac}-U_{dc}$  plane by keeping the  $U_{dc}/U_{ac}$  ratio constant, a sequence of the following transitions pattern-free planar - pattern-free quasihomotropic - cellular - parallel stripes - normal rolls were observed. The boundaries between various pattern types were typically not sharp; it might partially be due to the dependence on the sample history, or to the coexistence/superposition of neighbouring pattern types (e.g., superposition of planar stripes with normal rolls yielded a special herringbone pattern). The influence of  $U_{dc}$  on  $\sigma_{\perp}$  and  $\sigma_a/\sigma_{\perp}$  may certainly play a role here too.

### 6.3. Stochastic driving

Electroconvecting nematics are suitable materials also for investigating the influence of multiplicative noise on pattern formation in an extended system. In a sequence of experiments, a stochastic driving signal, synthesized

by superposing a deterministic (sinusoidal) voltage with a non-deterministic component (a white noise), was applied to MBBA and an increase of the conductive EC threshold as well as of the wave number with the noise amplitude was observed [176–178]. This effect was interpreted using the simple 1D model of EC. It was also shown that, besides the shift of the onset voltage, noise also delays the onset of EC (increases the growth time); moreover, it postpones the onset of turbulence [179,180]. Further experiments showed that colouring the noise, i.e., cutting its high-frequency components, the threshold increment of conductive EC reduces and can even turn to negative [181–184]. Thus, the effect of the noise may be tuned from suppressing pattern formation to promoting it, depending on the relation between the highest frequency of the noise and the cut-off frequency of the LC [183]. As a consequence, the response of conductive EC and dielectric EC on stochastic excitation is substantially different; in the latter case, the threshold dependence on the noise intensity is non-monotonic [185]. Differences between the behaviour of planar and homeotropic samples were also studied [186]. Noise also has an effect on the thresholds of further instabilities at high voltages in the nonlinear regime [184]. The influence of an additional magnetic field (which suppresses the additive noise related to director fluctuations) was also investigated [187]. It has to be noted that a pure stochastic excitation can also lead to the formation of EC patterns, which was proven for a homeotropic sample [188].

Another experimental approach for a stochastic driving was using square wave as the deterministic signal and a dichotomous Markovian noise (i.e., random jumps between two voltage values of opposite sign) as the non-deterministic component. Measurements on Mischung 5 indicated threshold variations and spatiotemporal fluctuation of the patterns [189]. The purely stochastic driving was analysed in more detail. Patterns appeared in the form of bursts above the DC threshold, but already below the deterministic (SQW) threshold voltage [190]. These bursts correspond to an on–off intermittency between the patterned and the initial homogeneous state. The probability distribution of the duration of the intermittent states was analysed and compared to theoretical simulations [191].

Theoretical description of the pattern formation under stochastic driving is a challenging task. The numerical tools used for calculations in the SM (harmonic expansions for the temporal behaviour) are not compatible with the applied non-deterministic voltages. Therefore, different theoretical approaches had to be developed based on lower dimension approximate models [191–196]. The methods and results are summarized in a review [46].

## 7. Dynamics of defects and embedded particles

We have seen in Section 4.3.1 that if the applied voltage reaches the Eckhaus limit, the regular roll structure becomes unstable against the formation of defects (dislocations). Figure 14(a) displays a pair of such defects. Defects play an important role also below the Eckhaus limit, in adjusting the wave vector of the pattern after changes in the control parameters ( $U$  and  $f$ ). For example, if the voltage and/or the frequency is altered from  $(U_0, f_0)$  to  $(U_1, f_1)$ , the wave vector should adjust itself from  $\mathbf{q}_0(U_0, f_0)$  to  $\mathbf{q}_1(U_1, f_1)$ . This change cannot occur momentarily; therefore, a temporary wave vector mismatch  $\Delta\mathbf{q} = \mathbf{q}_1 - \mathbf{q}_0$  develops, which relaxes to zero as time evolves. In extended systems, like in typical LC cells having a large ( $> 100$ ) aspect ratio,  $\mathbf{q}$  cannot change continuously. Instead, defects are created in pairs of opposite topological charge [197], which then move away from each other until they reach the cell boundary or annihilate with another defect of opposite topological charge. Motion of dislocations along the rolls (called *climbing*) adjusts the wavelength (i.e.,  $|\mathbf{q}|$ ) in small steps, while motion perpendicular to the rolls (called *gliding*) introduces small rotation of  $\mathbf{q}$  [197,198]. In order to resolve the wave vector mismatch, usually generation, motion and then disappearance of a large number of defects are required.

Dynamics of defects depends, besides the material parameters, on the mismatch  $\Delta\mathbf{q}$ . The weakly nonlinear analysis of the SM provides a relation between the mismatch and the velocity of isolated defects [197,199]. The velocity increases linearly with  $\Delta\mathbf{q}$ , except in the  $\Delta\mathbf{q} \rightarrow 0$  limit, where a logarithmic singularity occurs. Experimentally, studying defect motion requires different conditions for climbing and gliding. Climbing may be induced by changing the frequency and voltage simultaneously, with precautions to keep the relative excess voltage  $\Delta U/U$  the same for both frequencies [200,201]. Gliding could be provoked in homeotropic EC by rotating the sample in a symmetry-breaking magnetic field [202]. The velocity of defects or the temporal evolution of their number could experimentally be obtained from a time sequence of snapshots using specific algorithms for locating the position of the defects [200,202] and the logarithmic singularity could be justified. The same technique could be utilized to study the formation of chevrons (the superstructures formed by defect chains, see Section 4.3.1) [201,203].

The dislocations discussed above are localized defects; they have a well-defined core. There are, however, ‘long’ defects too (see Figure 14(c)), which are delocalized over several rolls into phase-jump lines; they occur frequently in the AR range either in planar or in homeotropic

samples [204]. Dynamics of similar, breather-like defects (having no singular core) has also been studied theoretically as well as experimentally in twisted nematic samples [205,206].

The prewavy pattern of the bent-core nematic CIP-bis10BB may form very spectacular temporary defect structures on the way to reduce the  $\mathbf{q}$ -mismatch: the knitting instability (Figure 24) [36]. Recently, a very similar scenario has been reported in another BCN and analysed carefully uncovering director distributions, the velocities and number of defects; just under the name of metastable chevrons of the in-plane normal rolls [150]. Based on the reported data, we assume that the different names cover the same structures.

Boundaries of zigzag structures and abnormal roll domains represent another type of defect: walls. Considerable theoretical efforts have been devoted to understand their formation and dynamics [113,207,208].

The optical contrast of the patterns seen in the microscope comes solely from the director modulation; flow or space charge distribution is not directly visible. However, flow can be revealed using tracer particles. Dust particles, often present in the samples, may serve as tracers; alternatively, colloidal particles (e.g., silica micro spheres) may be embedded into the LC. Tracer particles allow one to prove the presence of flow vortices in the plane perpendicular to the s-EC rolls; they repeatedly circle out of and then back into focus within the roll. Very recently, this was demonstrated in a low birefringence nematic; in addition, measuring the velocity of single particles allowed one to distinguish between electro-foretic motion (below  $U_c$ ) and motion due to EC [209]. The particles tended to form self-assembled chains, much longer than the wavelength of the conductive s-EC rolls; the onset of EC induced the undulation and thus an apparent shortening of these particle chains [209].

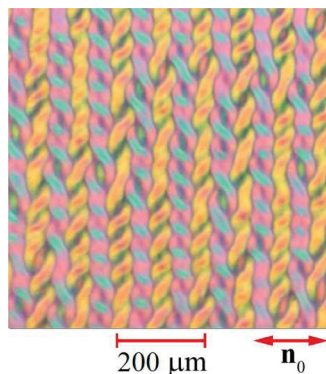


**Figure 24.** Snapshot of the knitting instability in the BCN CIP-bis10BB ( $d = 10 \mu\text{m}$ ) [36]. The double arrow indicates the initial director  $\mathbf{n}_0$ . Crossed polarizers; the light polarization is rotated from  $\mathbf{n}_0$  by  $15^\circ$ .

The transport properties of colloidal particles were investigated during s-EC in a wide voltage range in planar geometries [210,211]. At voltages moderately above the threshold, the particles were found to be trapped in a single convection roll exhibiting two different types of motion: rotation in the vortex flow and gliding along convection rolls. Increasing the voltage resulted in higher rotation frequency and higher gliding velocity. At high voltage excitation, in the presence of temporally fluctuating roll structure (i.e., entering into the defect chaos regime), the motion became with two-dimensional by the hopping of particles between neighbouring rolls. The particle transport perpendicular to the rolls exhibited diffusion character and could well be described by a stochastic model considering the rotation frequency of the particles, the roll width and the hopping probability [210]. At high voltage, two kinds of spatiotemporal chaos [87] could be detected: coexisting with defect turbulence also grid patterns may develop in clusters of varying size and shape [211]. Therefore, at a given location, a spatiotemporal intermittency, i.e., a random switching between disordered and ordered states, occurs. Trajectories of the particles were investigated and statistically analysed for both cases [211].

Embedding colloidal particles in the liquid crystal was also used in the homeotropic geometry, to study the soft mode turbulence [88,212]. The chaotic flow field-induced random motion of microparticles and the resulting non-thermal Brownian motion was studied. Two types of particle motion were found: the faster process was related to the rotation with the convection and hopping to neighbouring rolls; the slower one was described as a consequence of the slowly changing larger scale pattern dynamics of the soft mode turbulence. The particle diffusion could be described by non-Gaussian distribution of particle displacement, and the results were analysed by a generalized Langevin equation [212].

Particles were used to uncover the flow pattern of the prewavy pattern. In contrast to s-EC, the vortices in this ns-EC pattern are parallel to the substrates; the flow velocity has opposite direction in the neighbouring stripes of PW [108].

## 8. Summary/outlook

Reviewing the electric field-induced pattern formation in liquid crystals – whose study has a history of about a half century – necessarily might not be complete. For example, in the present review, we constrained ourselves to the electric field-induced patterns in the nematic phase only, even though patterns may exist in other, e.g., cholesteric and smectic phases as well.

We made an attempt to systematically overview the stability limits of the nematic system, i.e., the conditions, which lead to the appearance of patterns under an applied electric field. The crossover from the basic state into the pattern forming instability is the result of a delicate balance of the control, material and system parameters, which, in most cases, is theoretically well understood and described.

However, despite the huge knowledge accumulated during the past decades by investigating patterns in a large number of nematics and the great theoretical efforts performed aiming to understand the basic mechanisms and occasionally the fine details of the pattern formation, some questions still remained open. These questions are mostly related to nonstandard electroconvection.

Obvious examples are those patterns [e.g., the prewavy pattern or the patterns arising in (+ +) nematics], where the mechanism of pattern formation has not yet fully identified or only simplified, low-dimensional models have been proposed. We assume that the determinative processes of the complex phenomenon of pattern formation have already been identified. Some of them (director relaxation, viscous flow, space charge separation) are contained by the SM, some others (e.g., flexoelectricity, ionic migration/association/dissociation) have been additionally included as individual extensions (extended SM or WEM) and some have been modelled in an isotropic environment (ionic effects, injection and resulting electric field gradients). A unification of the theories by incorporating all these components and thus becoming able to provide most of the missing answers is a huge theoretical challenge; at the moment it is still a dream for the future.

The crossover between flexodomains and ns-EC longitudinal rolls upon increasing the frequency is another example for the unresolved problems. In FDs, flow is negligible, while in LR flow is important; nevertheless, both patterns have similar  $\mathbf{q}$  and in both of them flexoelectricity plays a determinative role. It is yet unclear, how the two patterns can be distinguished experimentally, or by other words, up to which  $f$  can the pattern be regarded as FDs (keeping in mind that at high  $f$ , the director relaxation surely induces flow). This question has recently been arisen concerning the interpretation of patterns observed in an oxadiazole compound [33,149]. We may, however, put the question another way: is it necessary to distinguish these two patterns or this intention is due to an artifact, a result of the shortcomings of various theoretical models used for the interpretation. Further experimental tests and theoretical considerations, including numerical simulations, might be necessary to obtain a comforting answer.

The present review aimed to summarize our knowledge about the stability limits (instability thresholds)

in electric field-induced pattern formation, as well as about what happens if one goes outside these limits. This knowledge is also vital if patterns are unwanted and should be avoided, since for that, the safest strategy is to remain in the stable region of the parameters. If, in a specific geometry, this requirement is not met, pattern formation seems to be unavoidable. Then, modification/adjustment of the parameters remains the only clue to push the system back to the safe side of the SLC. This may be performed by choosing another LC with more appropriate parameters, or by reducing the conductivity of the selected LC with proper additives (e.g., doping by nanoparticles), or via suppressing pattern formation by an additional, superposed field (e.g., by a DC bias).

## Disclosure statement

No potential conflict of interest was reported by the authors.

## Funding

This work has been supported by the Hungarian Scientific Research Fund (OTKA) [grant number NN110672].

## References

- [1] de Gennes PG, Prost J. The physics of liquid crystals. 2nd ed. Oxford: Clarendon Press; 1993.
- [2] Blinov LM, Chigrinov VG. Electrooptic effects in liquid crystal materials. Berlin–Heidelberg: Springer; 1994.
- [3] Buka Á, Éber, N. editors. Flexoelectricity in liquid crystals: theory, experiments and applications. London: Imperial College Press; 2012.
- [4] Hartshorne NH, Stuart A. Crystals and the polarising microscope. 4th ed. London: Edward Arnold; 1970.
- [5] Amm H, Stannarius R, Rossberg AG. Optical characterization of chevron texture formation in nematic electroconvection. *Physica D*. 1999;126:171–188.
- [6] Rasenat S, Hartung G, Winkler BL, et al. The shadowgraph method in convection experiments. *Exp Fluids*. 1989;7:412–420.
- [7] Trainoff SP, Cannell DS. Physical optics treatment of the shadowgraph. *Phys Fluids*. 2002;14:1340–1363.
- [8] Pesch W, Krekhov A. Optical analysis of spatially periodic patterns in nematic liquid crystals: diffraction and shadowgraphy. *Phys Rev E*. 2013;87:052504.
- [9] Buka A, de la Torre Juárez M, Kramer L, et al. Transient structures in the Fréedericksz transition. *Phys Rev A*. 1989;40:7427–7430.
- [10] Guyon E, Meyer R, Salan J. Domain structure in the nematic Freedericksz transition. *Mol Cryst Liq Cryst*. 1979;54:261–272.
- [11] Carr E. Domains due to magnetic fields in bulk samples of a nematic liquid crystal. *Mol Cryst Liq Cryst*. 1977;34:159–164.
- [12] Hurd AJ, Fraden S, Lonberg F, et al. Field-induced transient periodic structures in nematic liquid crystals: the splay Frederiks transition. *J Phys (Paris)*. 1985;46:905–918.

- [13] Fraden S, Hurd AJ, Meyer R, et al. Magnetic-field-induced alignment and instabilities in ordered colloids of tobacco mosaic virus. *J Phys (Paris) Colloq.* **1985**;46:C3-85–C3-114.
- [14] Winkler BL, Richter H, Rehberg I, et al. Nonequilibrium patterns in the electric-field-induced splay Freedericksz transition. *Phys Rev A.* **1991**;43:1940–1948.
- [15] Buka A, Kramer L. Theory of nonlinear transient patterns in the splay Fréedericksz transition. *Phys Rev A.* **1992**;45:5624–5631.
- [16] Buka A, Kramer L. Linear and non-linear transient patterns in the splay Freedericksz transition of nematics. *J Phys II (Paris).* **1992**;2:315–326.
- [17] Lonberg F, Fraden S, Hurd AJ, et al. Field-induced transient periodic structures in nematic liquid crystals: the twist-Fréedericksz transition. *Phys Rev Lett.* **1984**;52:1903–1906.
- [18] Srajer G, Fraden S, Meyer R. Field-induced nonequilibrium periodic structures in nematic liquid crystals: nonlinear study of the twist Frederiks transition. *Phys Rev A.* **1989**;39:4828–4834.
- [19] Sagues F, san Miguel M. Transient patterns in nematic liquid crystals: domain-wall dynamics. *Phys Rev A.* **1989**;39:6567–6572.
- [20] Grigutsch M, Klöpper N, Schmiedel H, et al. Transient structures in the twist Fredericksz transition of low-molecular-weight nematic liquid crystals. *Phys Rev E.* **1994**;49:5452–5461.
- [21] Frisken B, Palfy-Muhoray P. Electric-field-induced twist and bend Freedericksz transitions in nematic liquid crystals. *Phys Rev A.* **1989**;39:1513–1518.
- [22] Allender D, Frisken B, Palfy-Muhoray P. Theory of an electric field induced periodic phase in a nematic film. *Liq Cryst.* **1989**;5:735–738.
- [23] Lonberg F, Meyer RB. New ground state for the splay-Fréedericksz transition in a polymer nematic liquid crystal. *Phys Rev Lett.* **1985**;55:718–721.
- [24] Tamba M-G, Weissflog W, Eremin A, et al. Electro-optic characterization of a nematic phase formed by bent core mesogens. *Eur Phys J E.* **2007**;22:85–95.
- [25] Bobylev YuP, Pikin SA. Threshold piezoelectric instability in a liquid crystal. *Sov Phys JETP.* **1977**;45:195–198 [*Zh Eksp Teor Phys.* 1977;72:369–374].
- [26] Buka Á, Tóth-Katona T, Éber N, et al. Chapter 4, The role of flexoelectricity in pattern formation. In: Buka Á, Éber N, editors. *Flexoelectricity in liquid crystals. Theory, experiments and applications.* London: Imperial College Press; 2012, p. 101–135.
- [27] Krekhov A, Pesch W, Buka A. Flexoelectricity and pattern formation in nematic liquid crystals. *Phys Rev E.* **2011**;83:051706.
- [28] Terent'ev EM, Pikin SA. Nonlinear effects in a real flexoelectric structure. *Sov Phys JETP.* **1982**;56:587–590 [*Zh Eksp Teor Phys.* 1982;83:1038–1044].
- [29] Xu M-Y, Zhou M-j, Xiang Y, et al. Domain structures as optical gratings controlled by electric field in a bent-core nematic. *Opt Expr.* **2015**;23:15224.
- [30] Salamon P, Éber N, Buka Á, et al. Magnetic control of flexoelectric domains in a nematic fluid. *Soft Matter.* **2014**;10:4487–4497.
- [31] Buka Á, Toth-Katona T, Éber N, et al. Chapter 4, The role of flexoelectricity in pattern formation. In: Buka Á, Éber N, editors. *Flexoelectricity in liquid crystals. Theory, experiments and applications.* London: Imperial College Press; 2012, p. 101–135.
- [32] Salamon P, Éber N, Krekhov A, et al. Flashing flexodomains and electroconvection rolls in a nematic liquid crystal. *Phys Rev E.* **2013**;87:032505.
- [33] Kaur S, Panov VP, Greco C, et al. Flexoelectricity in an oxadiazole bent-core nematic liquid crystal. *Appl Phys Lett.* **2014**;105:223505.
- [34] Jákli A. Liquid crystals of the twenty-first century – nematic phase of bent-core molecules. *Liq Cryst Rev.* **2013**;1:65–82.
- [35] Le KV, Araoka F, Fodor-Csorba K, et al. Flexoelectric effect in a bent-core mesogen. *Liq Cryst.* **2009**;36:1119–1124.
- [36] Wiant DB, Gleeson JT, Éber N, et al. Non-standard electroconvection in a bent core nematic. *Phys Rev E.* **2005**;72:041712.
- [37] Buka Á, Éber N, Fodor-Csorba K, et al. Physical properties of a bent-core nematic liquid crystal and its mixtures with calamitic molecules. *Phase Transitions.* **2012**;85:872–887.
- [38] Tadapatri P, Krishnamurthy KS, Weissflog W. Patterned flexoelectric instability in a bent-core nematic liquid crystal. *Soft Matter.* **2012**;8:1202–1214.
- [39] Xiang Y, Liu Y-k, Buka Á, et al. Electric-field-induced patterns and their temperature dependence in a bent-core liquid crystal. *Phys Rev E.* **2014**;89:012502.
- [40] Krishnamurthy KS. Spatiotemporal character of the Bobylev-Pikin flexoelectric instability in a twisted nematic bent-core liquid crystal exposed to very low frequency fields. *Phys Rev E.* **2014**;89:052508.
- [41] Buka Á, Éber N, Pesch W, et al. Convective patterns in liquid crystals driven by electric field. In: Golovin AA, Nepomnyashchy AA, editors. *Self assembly, pattern formation and growth phenomena in nano-systems.* Dordrecht: Springer; 2006. p. 55–82.
- [42] Kochowska E, Németh Sz, Pelzl G, et al. Electroconvection with and without the Carr–Helfrich effect in a series of nematic liquid crystals. *Phys Rev E.* **2004**;70:011711.
- [43] Blinov LM, Barnik MI, Trufanov AN. Modern classification of electrohydrodynamic instabilities in the nematic phase. *Mol Cryst Liq Cryst.* **1982**;89:47–55.
- [44] Pikin SA. *Structural transformations in liquid crystals.* New York: Gordon and Breach Science; 1991.
- [45] Kramer L, Pesch W. Electrohydrodynamic instabilities in nematic liquid crystals. In: Buka Á, Kramer L, editors. *Pattern formation in liquid crystals.* New York: Springer; 1996. p. 221–256.
- [46] Pesch W, Behn U. Electrohydrodynamic convection in nematics. In: Busse FH, Müller SC, editors. *Evolution of spontaneous structures in dissipative continuous systems (Lecture Notes in Physics, Vol. 55).* Berlin–Heidelberg: Springer; 1998. p. 335–383.
- [47] Kramer L, Pesch W. Electrohydrodynamics in nematics. In: Dunmur DA, Fukuda A, Luckhurst GR, editors. *Physical properties of nematic liquid crystals.* London: Inspec; 2001. p. 441–454.
- [48] Buka Á, Éber N, Pesch W, Kramer L. Isotropic and anisotropic electroconvection. *Phys Rep.* **2007**;448:115–132.

- [49] Williams R. Domains in liquid crystals. *J Chem Phys.* **1963**;39:384–388.
- [50] Carr EF. Influence of electric fields on the molecular alignment in the liquid crystal p-(anisalamino)-phenyl acetate. *Mol Cryst Liq Cryst.* **1969**;7:253–268.
- [51] Helfrich W. Conduction-induced alignment of nematic liquid crystals: basic model and stability considerations. *J Chem Phys.* **1969**;51:4092–4105.
- [52] Bodenschatz E, Zimmermann W, Kramer L. On electrically driven pattern-forming instabilities in planar nematics. *J Phys France.* **1988**;49:1875–1899.
- [53] Pesch W, Kramer L. General mathematical description of pattern-forming instabilities. In: Buka Á, Kramer L, editors. *Pattern formation in liquid crystals.* New York: Springer; 1996. p. 69–90.
- [54] Krekhov A, Pesch W, Éber N, et al. Nonstandard electroconvection and flexoelectricity in nematic liquid crystals. *Phys Rev E.* **2008**;77:021705.
- [55] Treiber M, Kramer L. Bipolar electrodiffusion model for electroconvection in nematics. *Mol Cryst Liq Cryst.* **1995**;261:311–326.
- [56] Kai S, Hirakawa K. Phase diagram of dissipative structures in the nematic liquid crystal under a.c.-field. *Solid State Commun.* **1976**;18:1573–1577.
- [57] Dennin M, Treiber M, Kramer L, et al. Origin of traveling rolls in electroconvection of nematic liquid crystals. *Phys Rev Lett.* **1996**;76:319–322.
- [58] May M, Schöpf W, Rehberg I, et al. Transition from longitudinal to transversal patterns in an anisotropic system. *Phys Rev E.* **2008**;78:046215.
- [59] Rehberg I, Rasenat S, de la Torre Juárez M, et al. Thermally induced hydrodynamic fluctuations below the onset of electroconvection. *Phys Rev Lett.* **1991**;67:596–599.
- [60] Éber N, Palomares LO, Salamon P, et al. Temporal evolution and alternation of mechanisms of electric field induced patterns at ultra-low-frequency driving. *Phys Rev E.* **2012**;86:021702.
- [61] Amm H, Grigutsch M, Stannarius R. Optical characterization of electroconvection in nematics. *Mol Cryst Liq Cryst.* **1998**;320:11–27.
- [62] Éber N, Rozanski SA, Németh Sz, et al. Decay of spatially periodic patterns in a nematic liquid crystal. *Phys Rev E.* **2004**;70:061706.
- [63] Kai S, Hirakawa K. Successive transitions in electrohydrodynamic instabilities of nematics. *Prog Theor Phys Suppl.* **1978**;64:212–243.
- [64] Ramou E, Zenginoglou HM, Papadopoulos PL. On an objective experimental method for the determination of the electrohydrodynamic instability thresholds in a nematic liquid crystal. *Liq Cryst.* **2014**;41:1–8.
- [65] Éber N, Salamon P, Buka Á. Competition between electric field induced equilibrium and non-equilibrium patterns at low frequency driving in nematics. In: Buša J, Hnatič M, Kopčanský P, editors. *13th Small Triangle Meeting on Theoretical Physics*; 2011 Nov 14–16; Stará Lesná, Slovakia. Košice: IEP SAS; 2012. p. 56–63.
- [66] Tóth-Katona T, Éber N, Buka Á. Temporal response to harmonic driving in electroconvection. *Phys Rev E.* **2011**;83:061704.
- [67] Tóth-Katona T, Éber N, Buka Á. Flexoelectricity in electroconvection. *Mol Cryst Liq Cryst.* **2009**;511:11–24.
- [68] Rehberg I, Rasenat S, Fineberg J, et al. Temporal modulation of traveling waves. *Phys Rev Lett.* **1988**;61:2449–2452.
- [69] Rehberg I, Rasenat S, Steinberg V. Traveling waves and defect-initiated turbulence in electroconvecting nematics. *Phys Rev Lett.* **1989**;62:756–759.
- [70] Treiber M, Éber N, Buka Á, et al. Travelling waves in electroconvection of the Nematic Phase 5: a test of the weak electrolyte model. *J Phys II France.* **1997**;7:649–661.
- [71] Acharya G, Dangelmayr G, Gleeson J, et al. Steady state–Hopf mode interaction at the onset of electroconvection in the nematic liquid crystal Phase V. *Int J Mol Sci.* **2011**;12:4488–4503.
- [72] Pucci G, Lysenko D, Provenzano C, et al. Patterns of electro-convection in planar-periodic nematic cells. *Liq Cryst.* **2016**;43:216–221.
- [73] Kaoui B, Guckenberger A, Krekhov A, et al. Coexistence of stable branched patterns in anisotropic inhomogeneous systems. *New J Phys.* **2015**;17:103015.
- [74] Rudroff S, Zhao H, Kramer L, et al. Secondary instabilities form a codimension-2 point accompanied by a homoclinic bifurcation. *Phys Rev Lett.* **1998**;81:4144–4147.
- [75] Hirata S, Tako T. Effect of cell width on the structure of Williams domain. *Jpn J Appl Phys Part 2.* **1982**;21:L607–L609.
- [76] Binks DJ, Mullin T. Cell number selection in electrohydrodynamic convection in liquid crystals. *Proc R Soc Lond A.* **1997**;453:2109–2122.
- [77] Mullin T, Tavener SJ, Blake GI. Electrohydrodynamic convection in small aspect ratio devices. *J Non-Newtonian Fluid Mech.* **2004**;119:61–69.
- [78] Katranchev B, Naradikian H, Keskinova E, et al. Electroconvective dendrites in nematic phases having short range smectic order exhibited by the 4,n-alkoxybenzoic acids. *Liq Cryst.* **2004**;31:1663–1676.
- [79] Kai S, Yamaguchi K, Hirakawa K. Observation of flow figures in nematic liquid crystal MBBA. *Jpn J Appl Phys Part 1.* **1975**;14:1653–1658.
- [80] Huh J-H, Kai S. Electroconvection in nematic liquid crystals in Hele-Shaw cells. *Phys Rev E.* **2003**;68:042702.
- [81] Bohatsch H, Stannarius R. Frequency-induced structure transition of nematic electroconvection in twist cells. *Phys Rev E.* **1999**;60:5591–5599.
- [82] Buka A, Dressel B, Otowski W, et al. Electroconvection in nematic liquid crystals with positive dielectric and negative conductivity anisotropy. *Phys Rev E.* **2002**;66:051713.
- [83] Zhang B, Kitzerow H. Pattern formation in a nematic liquid crystal mixture with negative anisotropy of the electric conductivity – a long-known system with ‘inverse’ light scattering revisited. *J Phys Chem B.* **2016**. DOI: 10.1021/acs.jpcc.6b05080.
- [84] Buka Á, Tóth P, Éber N, et al. Electroconvection in homeotropically aligned nematics. *Phys Rep.* **2000**;337:157–169.
- [85] Hertrich A, Decker W, Pesch W, et al. The electrohydrodynamic instability in homeotropic nematic layers. *J Phys II (Paris).* **1992**;2:1915–1930.
- [86] Éber N, Németh Sz, Rossberg AG, et al. Magnetic field effects on the thresholds of a sequence of transitions in

- the electroconvection of a homeotropic nematic liquid crystal. *Phys Rev E*. **2002**;66:036213.
- [87] Hidaka Y, Oikawa N. Chaos and spatiotemporal chaos in convective systems. *Forma*. **2014**;29:29–32.
- [88] Hidaka Y, Tamura K, Kai S. Soft-mode turbulence in electroconvection of nematics. *Prog Theor Phys Suppl*. **2006**;161:1–11.
- [89] Richter H, Klöpper N, Hertrich A, et al. Electroconvection in a homeotropic nematic under the influence of a magnetic field. *Europhys Lett*. **1995**;30:37–42.
- [90] Kai S, Hayashi K-i, Hidaka Y. Pattern forming instability in homeotropically aligned liquid crystals. *J Phys Chem*. **1996**;100:19007–19016.
- [91] Nugroho F, Hidaka Y, Ueki T, et al. Transient mode selections in soft-mode turbulence by controlling the Nambu-Goldstone modes. *J Phys Soc Jpn*. **2012**;81:024004.
- [92] Iino M, Hidaka Y, Nugroho F. Responses of spatiotemporal chaos to oscillating forces. *Phys Rev E*. **2015**;92:012916.
- [93] Stannarius R, Heuer J. Electroconvection in nematics above the splay Fréedericksz transition. *Eur Phys J E*. **2007**;24:27–33.
- [94] Heuer J, Stannarius R, Tamba MG, et al. Longitudinal and normal electroconvection rolls in a nematic liquid crystal with positive dielectric and negative conductivity anisotropy. *Phys Rev E*. **2008**;77:056206.
- [95] Goscianski M, Léger L. Electrohydrodynamic instabilities above a nematic to smectic A (or C) transition. *J Phys (Paris) Coll*. **1975**;36:C1-231–C1-235.
- [96] Blinov LM, Barnik MI, Lazareva VT, et al. Electrohydrodynamic instabilities in the liquid crystalline phases with smectic ordering. *J Phys (Paris) Coll*. **1979**;40:C3-263–C3-268.
- [97] Tóth-Katona T, Cauquil-Vergnes A, Éber N, et al. Non-standard electroconvection with Hopf-bifurcation in a nematic with negative electric anisotropies. *Phys Rev E*. **2007**;75:066210.
- [98] Nakagawa M, Akahane T. A new type of electrohydrodynamic instability in nematic liquid crystals with positive dielectric anisotropy. I. The existence of the charge injection and the diffusion current. *J Phys Soc Jpn*. **1983**;52:3773–3781.
- [99] Kumar P, Heuer J, Tóth-Katona T, et al. Convection-roll instability in spite of a large stabilizing torque. *Phys Rev E*. **2010**;81:020702(R).
- [100] Aguirre LE, Anardo E, Éber N, et al. Regular structures in 5CB liquid crystals under the joint action of ac and dc voltages. *Phys Rev E*. **2012**;85:041703.
- [101] Rjuntsev EI, Polushin SG. Electrohydrodynamic instabilities in nematic liquid crystals with large positive dielectric anisotropy. *Liq Cryst*. **1993**;13:623–628.
- [102] Trufanov AN, Barnik MI, Blinov LM, et al. Electrohydrodynamic instability in homeotropically oriented layers of nematic liquid crystals. *Sov Phys JETP*. **1981**;53:355–361 [*Zh Eksp Teor Fiz*. **1981**;80:704–715].
- [103] Rout DK, Choudhary RNP. Electrohydrodynamic instability in some nematic cyanobiphenyls in an a.c. electric field. *Liq Cryst*. **1989**;4:393–398.
- [104] Barnik MI, Blinov LM, Pikin SA, et al. Instability mechanism in the nematic and isotropic phases of liquid crystals with positive dielectric anisotropy. *Sov Phys JETP*. **1977**;45:396–398 [*Zh Eksp Teor Fiz*. **1977**;72:756–761].
- [105] Nakagawa M, Akahane T. A new type of electrohydrodynamic instability in nematic liquid crystals with positive dielectric anisotropy. II. Theoretical treatment. *J Phys Soc Jpn*. **1983**;52:3782–3789.
- [106] Petrescu P, Giurgea M. A new type of domain structure in nematic liquid crystals. *Phys Lett A*. **1976**;59:41–42.
- [107] Huh J-H, Hidaka Y, Yusuf Y, et al. Prewavy pattern: a director-modulation structure in nematic liquid crystals. *Mol Cryst Liq Cryst*. **2001**;364:111–122.
- [108] Huh J-H, Yusuf Y, Hidaka Y, et al. Prewavy instability of nematic liquid crystals in a high-frequency electric field. *Phys Rev E*. **2002**;66:031705.
- [109] Éber N, Buka Á. Electroconvection in homeotropic nematic liquid crystals. *Phase Transitions*. **2005**;78:433–442.
- [110] Petrov M, Katranchev B, Keskinova E, et al. The electroconvection in dimeric nematic liquid crystals. *J Optoelectr Adv Mater*. **2007**;9:438–441.
- [111] Katranchev B, Petrov M. Prewavy electrohydrodynamic instability in dimeric nematic liquid crystals with short range smectic ‘C’ order. *Compt Rend Acad Bulg Sci*. **2009**;62:329–334.
- [112] Yusuf Y, Hidaka Y, Kai S. Dynamical behavior of prewavy pattern near nematic-isotropic transition. *J Phys Soc Jpn*. **2013**;82:044601.
- [113] Komineas S, Zhao H, Kramer L. Modulated structures in electroconvection in nematic liquid crystals. *Phys Rev E*. **2003**;67:031701.
- [114] Tanaka S, Dhara S, Sadashiva BK, et al. Alternating twist structures formed by electroconvection in the nematic phase of an achiral bent-core molecule. *Phys Rev E*. **2008**;77:041708.
- [115] Tanaka S, Takezoe H, Éber N, et al. Electroconvection in nematic mixtures of bent-core and calamitic molecules. *Phys Rev E*. **2009**;80:021702.
- [116] Tadapatri P, Krishnamurthy KS, Weissflog W. Multiple electroconvection scenarios in a bent-core nematic liquid crystal. *Phys Rev E*. **2010**;82:031706.
- [117] Tadapatri P, Hiramath US, Yelamaggad CV, et al. Patterned electroconvective states in a bent-core nematic liquid crystal. *J Phys Chem B*. **2010**;114:10–21.
- [118] Tadapatri P, Krishnamurthy KS. Competing instability modes in an electrically driven bent-core nematic liquid crystal. *J Phys Chem B*. **2012**;116:782–793.
- [119] Salamon P, Éber N, Buka Á, et al. Dielectric properties of mixtures of a bent-core and a calamitic liquid crystal. *Phys Rev E*. **2010**;81:031711.
- [120] Kumar P, Hiremath US, Yelamaggad CV, et al. Electroconvection in a homeotropic bent-rod nematic liquid crystal beyond the dielectric inversion frequency. *J Phys Chem B*. **2008**;112:9753–9760.
- [121] Xiang Y, Zhou M-j, Xu M-Y, et al. Unusual polarity-dependent patterns in a bent-core nematic liquid crystal under low-frequency ac field. *Phys Rev E*. **2015**;91:042501.
- [122] Joets A, Ribotta R. Hydrodynamic transitions to chaos in the convection of an anisotropic fluid. *J Phys (Paris)*. **1986**;47:595–606.

- [123] Kai S, Zimmermann W, Andoh M. Turbulence I – turbulence II transition in electrohydrodynamic convection. *Mod Phys Lett B*. 1990;4:767–774.
- [124] Carbone V, Scaramuzza N, Versace C. Multifractal structures in electro-convective turbulence. *Physica D*. 1997;106:314–326.
- [125] Lucchetta DE, Scaramuzza N, Strangi G, et al. Impurities in nematic liquid crystal samples inducing changes in the DSM1–DSM2 transition phase diagram. *Liq Cryst*. 2000;27:277–281.
- [126] Orsay Liquid Crystal Group. AC and DC regimes of the electrohydrodynamic instabilities in nematic liquid crystals. *Mol Cryst Liq Cryst*. 1971;12:251–266.
- [127] Rossberg AG, Kramer L. Pattern formation from defect chaos – a theory of chevrons. *Physica D*. 1998;115:19–28.
- [128] Ribotta R, Joets A, Lei L. Oblique roll instability in an electroconvective anisotropic fluid. *Phys Rev Lett*. 1986;56:1595–1597.
- [129] Plaut E, Decker W, Rossberg AG, et al. New symmetry breaking in nonlinear electroconvection of nematic liquid crystals. *Phys Rev Lett*. 1997;79:2367–2370.
- [130] Rossberg AG, Éber N, Buka Á, et al. Abnormal rolls and regular arrays of disclinations in homeotropic electroconvection. *Phys Rev E Rap Comm*. 2000;61:R25–R28.
- [131] Rossberg AG, Hertrich A, Kramer L, et al. Weakly nonlinear theory of pattern-forming systems with spontaneously broken isotropy. *Phys Rev Lett*. 1996;76:4729–4732.
- [132] Plaut E, Pesch W. Extended weakly nonlinear theory of planar nematic convection. *Phys Rev E*. 1999;59:1747–1769.
- [133] Richter H, Buka Á, Rehberg I. On the optical characterization of convection patterns in homeotropically aligned nematics. *Mol Cryst Liq Cryst Sci Tech Sect A Mol Cryst Liq Cryst*. 1994;251:181–189.
- [134] Huh J-H, Hidaka Y, Kai S. Observation and determination of abnormal rolls and abnormal zigzag rolls in electroconvection in homeotropic liquid crystals. *Phys Rev E*. 1998;58:7355–7358.
- [135] Huh J-H, Hidaka Y, Rossberg AG, et al. Pattern formation of chevrons in the conduction regime in homeotropically aligned liquid crystals. *Phys Rev E*. 2000;61:2769–2776.
- [136] Buka Á, Dressel B, Kramer L, et al. Direct transition to electroconvection in a homeotropic nematic liquid crystal. *Chaos*. 2004;14:793–802.
- [137] Kochowska E, Éber N, Otowski W., et al. Square patterns and their dynamics in electroconvection. *Mol Cryst Liq Cryst*. 2005;435:243–253.
- [138] Katranchev B, Naradikian H, Keskinova E, et al. The electroconvection in nematic liquid crystals with short range smectic C order and negative electroconductivity anisotropy. *J Phys Conf Ser*. 2010;253:12062.
- [139] Dennin M, Ahlers G, Cannell DS. Chaotic localized states near the onset of electroconvection. *Phys Rev Lett*. 1996;77:2475–2478.
- [140] Hertrich A, Pesch W, Gleeson JT. Electrohydrodynamic convection with destabilizing magnetic field. *Europhys Lett*. 1996;34:417–422.
- [141] Gleeson JT. Onset of electroconvection in nematic liquid crystals with parallel magnetic field. *Phys Rev E*. 1996;54:6424–6429.
- [142] Gleeson JT. Dendritic growth of electrohydrodynamic convection in a nematic liquid crystal. *Nature*. 1997;385:511–513.
- [143] Gheorghii N, Gleeson JT. Length and speed selection in dendritic growth of electrohydrodynamic convection in a nematic liquid crystal. *Phys Rev E*. 2002;66:051710.
- [144] Dressel B, Pesch W. Competition between electroconvection and Fréedericksz distortions in nematic liquid crystals with slightly positive dielectric anisotropy. *Phys Rev E*. 2003;67:031707.
- [145] Krishnamurthy KS, Kumar P, Vijay Kumar M. Polarity-sensitive transient patterned state in a twisted nematic liquid crystal driven by very low frequency fields. *Phys Rev E*. 2013;87:022504.
- [146] Éber N, Salamon P, Fekete BA, et al. Suppression of spatially periodic patterns by dc voltage. *Phys Rev E*. 2016;93:042701.
- [147] Barnik MI, Blinov LM, Grebenkin MF, et al. Electrohydrodynamic instability in nematic liquid crystals. *Sov Phys JETP*. 1976;42:550–553 [*Zh Eksp Teor Fiz*. 1975;69:1080–1087].
- [148] Petrov M, Keskinova E, Katranchev B. The electroconvection in the nematic liquid crystals with short range smectic C order. *J Mol Liq*. 2008;138:130–138.
- [149] Kaur S, Belaissaoui A, Goodby JW, et al. Nonstandard electroconvection in a bent-core oxadiazole material. *Phys Rev E*. 2011;83:041704.
- [150] Krishnamurthy KS, Tadapatri P, Viswanath P. Dislocations and metastable chevrons in the electroconvective inplane normal roll state of a bent core nematic liquid crystal. *Soft Matter*. 2014;10:7316–7327.
- [151] Xiang Y, Goodby JW, Görtz V, et al. Revealing the uniaxial to biaxial nematic liquid crystal phase transition via distinctive electroconvection. *Appl Phys Lett*. 2009;94:193507.
- [152] De Jeu WH, Gerritsma CJ, Van Zanten P, et al. Relaxation of the dielectric constant and electrohydrodynamic instabilities in a liquid crystal. *Phys Lett*. 1972;39A:355–356.
- [153] Krishnamurthy KS, Kumar P. Effect of waveform of the driving field on electroconvection near the dielectric inversion frequency. *Phys Rev E*. 2016;93:022706.
- [154] Urbanski M, Kinkead B, Qi H, et al. Electroconvection in nematic liquid crystals via nanoparticle doping. *Nanoscale*. 2010;2:1118–1121.
- [155] Tóth-Katona T, Éber N, Buka Á, et al. Flexoelectricity and competition of time scales in electroconvection. *Phys Rev E*. 2008;78:036306.
- [156] Derfel G. Numerical study of ionic current in dielectric liquid layer subjected to ac voltage. *J Mol Liq*. 2009;144:59–64.
- [157] Freire FCM, Barbero G, Scalerandi M. Electrical impedance for an electrolytic cell. *Phys Rev E*. 2006;73:051202.
- [158] Omaira AE. Bent core nematics. Alignment and electro-optic effects [PhD dissertation]. Gothenburg (Sweden): University of Gothenburg; 2013.
- [159] John T, Stannarius R. Preparation of subharmonic patterns in nematic electroconvection. *Phys Rev E*. 2004;70:025202(R).
- [160] Low J, Hogan SJ. Standard and nonstandard nematic electrohydrodynamic convection in the presence of

- asymmetric ac electric fields. *Phys Rev E*. 2008;78:41706.
- [161] Heuer J, Stannarius R, John T. Reentrant EHC patterns under superimposed square wave excitation. *Mol Cryst Liq Cryst*. 2006;449:11–19.
- [162] Stannarius R, Heuer J, John T. Fundamental relations between the symmetry of excitation and the existence of spatiotemporal subharmonic structures in a pattern-forming dynamic system. *Phys Rev E*. 2005;72:066218.
- [163] Heuer J, John T, Stannarius R. Time reversal of the excitation wave form in a dissipative pattern-forming system. *Phys Rev E*. 2008;78:036218.
- [164] Joets A, Ribotta R. Localized, time-dependent state in the convection of a nematic liquid crystal. *Phys Rev Lett*. 1988;60:2164–2167.
- [165] Tu Y. Worm structure in the modified Swift–Hohenberg equation for electroconvection. *Phys Rev E*. 1997;56:R3765–R3768.
- [166] Riecke H, Granzow GD. Localization of waves without bistability: worms in nematic electroconvection. *Phys Rev Lett*. 1998;81:333–336.
- [167] Bisang U, Ahlers G. Bifurcation to worms in electroconvection. *Phys. Rev. E*. 1999;60:3910.
- [168] John T, Heuer J, Stannarius R. Influence of excitation wave forms and frequencies on the fundamental time symmetry of the system dynamics, studied in nematic electroconvection. *Phys Rev E*. 2005;71:056307.
- [169] Pietschmann D, John T, Stannarius R. Nematic electroconvection under time-reversed excitation. *Phys Rev E*. 2010;82:046215.
- [170] Salamon P, Éber N, Fekete B, et al. Inhibited pattern formation by asymmetrical high-voltage excitation in nematic fluids. *Phys Rev E*. 2014;90:022505.
- [171] Krekhov A, Decker W, Pesch W, et al. Patterns driven by combined ac and dc electric fields in nematic liquid crystals. *Phys Rev E*. 2014;89:052507.
- [172] Éber N, Salamon P, Fekete B, et al. Electroconvection in a nematic liquid crystal under superposed ac and dc electric voltages. In: Buša J, Hnatič M, Kopčanský P, editors. 15th Small triangle meeting on theoretical physics; 2013 Oct 27–30; Stará Lesná, Slovakia. Košice: IEP SAS; 2014. p. 46–51.
- [173] Marinov Y, Petrov AG, Hinov HP. On a simple way for obtaining important material constants of a nematic liquid crystal: longitudinal flexoelectric domains under the joint action of dc and ac voltages. *Mol Cryst Liq Cryst*. 2006;449:33.
- [174] Batyrshin ES, Krekhov AP, Skaldin OA, et al. Phase synchronization of the hydrodynamic and orientational modes during electroconvection in a nematic liquid crystal. *Tech Phys Lett*. 2014;40:1095–1097 [Pisma Zh Tekh Fiz. 2014;40:14–21].
- [175] Fekete BA. Patterns induced by superposition of low frequency AC and DC voltages in nematic liquid crystals [MSc thesis, in Hungarian]. Budapest: Budapest University of Technology and Economics; 2016.
- [176] Kai S, Kai T, Takata M, et al. Effect of the white noise on electrohydrodynamic transitions in nematics. *J Phys Soc Jpn*. 1979;47:1379–1380.
- [177] Kawakubo T, Yanagita A, Kabashima S. External noise effect on the onset of Williams domain in nematic liquid crystals. *J Phys Soc Jpn*. 1981;50:1451–1456.
- [178] Huh J-H. Noise-induced electrohydrodynamic patterns in nematic liquid crystals. *J Phys Soc Jpn*. 2007;76:033001.
- [179] Brand HR, Kai S, Wakabayashi S. External noise can suppress the onset of spatial turbulence. *Phys Rev Lett*. 1985;54:55–557.
- [180] Kai S, Fukunaga H, Brand HR. Structure changes induced by external multiplicative noise in the electrohydrodynamic instability of nematic liquid crystals. *J Stat Phys*. 1989;54:1133–1152.
- [181] Kai S, Fukunaga H, Brand HR. Experimental study on threshold shifts and structure changes due to external multiplicative noise in nematic liquid crystals. *J Phys Soc Jpn*. 1987;56:3759–3762.
- [182] Huh J-H, Kai S. Noise effects on threshold of electrohydrodynamic convection in nematic liquid crystals. *J Phys Soc Jpn*. 2008;77:083601.
- [183] Huh J-H. Noise-induced threshold shift and pattern formation in electroconvection by controlling characteristic time scales. *Phys Rev E*. 2011;84:025302(R).
- [184] Huh J-H, Kai S. Colored noise-induced threshold shifts and phase diagrams in electroconvections. *J Phys Soc Jpn*. 2014;83:063601.
- [185] Huh J-H, Kuribayashi A, Kai S. Noise-controlled pattern formation and threshold shift for electroconvection in the conduction and dielectric regimes. *Phys Rev E*. 2009;80:066304.
- [186] Huh J-H, Kuribayashi A, Kai S. Difference in noise-induced threshold shift between planar and homeotropic electroconvections in nematic liquid crystals. *J Phys Soc Jpn*. 2009;78:083601.
- [187] Huh J-H. Multiplicative noise effects on electroconvection in controlling additive noise by a magnetic field. *Phys Rev E*. 2015;92:062504.
- [188] Huh J-H, Kai S. Pure noise-induced pattern formations in a nematic liquid crystal. *J Phys Soc Jpn*. 2009;78:043601.
- [189] Amm H, Behn U, John T, et al. Electrohydrodynamic convection in nematics under stochastic excitation. *Mol Cryst Liq Cryst*. 1997;304:525–530.
- [190] John Th, Stannarius R, Behn U. On-off intermittency in stochastically driven electrohydrodynamic convection in nematics. *Phys Rev Lett*. 1999;83:749–752.
- [191] John T, Behn U, Stannarius R. Fundamental scaling laws of on-off intermittency in a stochastically driven dissipative pattern-forming system. *Phys Rev E*. 2002;65:046229.
- [192] Behn U, Müller R. Electrohydrodynamic instabilities in nematic liquid crystals driven by a dichotomous stochastic voltage. *Phys Lett*. 1985;113A:85–88.
- [193] Müller R, Behn U. Electrohydrodynamic instabilities in nematic liquid crystals under dichotomous parametric modulation. *Z Phys B Condens Matter*. 1987;69:185–192.
- [194] Müller R, Behn U. EHD instabilities in nematics driven by dichotomous noise: Stability criteria and influence of free boundary conditions. *Z Phys B Condens Matter*. 1990;78:229–234.
- [195] Lange A, Müller R, Behn U. Oblique rolls in nematic liquid crystals driven by stochastic fields: one-dimensional theory including the flexoeffect and three-dimensional theory. *Z Phys B Condens Matter*. 1996;100:477–488.

- [196] Behn U, Lange A, John Th. Electrohydrodynamic convection in liquid crystals driven by multiplicative noise: sample stability. *Phys Rev E*. **1998**;58:2047–2060.
- [197] Bodenschatz E, Pesch W, Kramer L. Structure and dynamics of dislocations in anisotropic pattern-forming systems. *Physica D*. **1988**;32:135–145.
- [198] Nasuno S, Takeuchi S, Sawada Y. Motion and interaction of dislocations in electrohydrodynamic convection of nematic liquid crystals. *Phys Rev A*. **1989**;40:3457–3460.
- [199] Pismen LM, Rodriguez JD. Mobility of singularities in the dissipative Ginzburg–Landau equation. *Phys Rev A*. **1990**;42:2471–2474.
- [200] Rasenat S, Steinberg V, Rehberg I. Experimental studies of defect dynamics and interaction in electrohydrodynamic convection. *Phys Rev A*. **1990**;42:5998–6008.
- [201] Kai S, Chizumi N, Kohno M. Spatial and temporal behavior of pattern formations and defect motions in the electrohydrodynamic instability of nematic liquid crystals. *Phys Rev A*. **1989**;40:6554–6572.
- [202] Tóth P, Éber N, Bock TM, et al. Dynamics of defects in electroconvection patterns. *Europhys Lett*. **2002**;57:824–830.
- [203] Scheuring M, Kramer L, Peinke J. Formation of chevrons in the dielectric regime of electroconvection in nematic liquid crystals. *Phys Rev E*. **1998**;58:2018–2026.
- [204] Buka Á, Börzsönyi T, Éber N, et al. Patterns in the bulk and at the interface of liquid crystals. In: Reguera D, Bonilla LL, Rubi J-M, editors. *Coherent Structures in Complex Systems: Selected Papers of the XVII Sitges Conference on Statistical Mechanics*; 2000 June 5–9; Sitges, Barcelona, Spain. Berlin–Heidelberg: Springer; 2001. p. 298–318 (Lecture Notes in Physics 567).
- [205] Skaldin OA, Delev VA, Shikhovtseva ES. Asymmetry of the time dynamics of breathers in the electroconvection twist structure of a nematic. *JETP Lett*. **2013**;97:92–97 [*Pisma v ZhETF*. 2013;97:98–103].
- [206] Skaldin OA, Delev VA, Shikhovtseva ES, et al. Breather-like defects and their dynamics in the one-dimensional roll structure of twisted nematics. *J Exp Theor Phys*. **2015**;121:1082–1095 [*Zh Eksp Teor Fiz*. 2015;148:1232–1247].
- [207] Zhao H, Kramer L. Zigzag structures and domain walls in electroconvection of nematic liquid crystal. *Phys Rev E*. **2000**;62:5092–5100.
- [208] Krekhov A, Dressel B, Pesch W, et al. Spatiotemporal complexity of electroconvection patterns in nematic liquid crystals. *Phys Rev E*. **2015**;92:062510.
- [209] Nishioka Y, Kobayashi F, Sakurai N, et al. Microscopic characterisation of self-assembled colloidal particles in electrohydrodynamic convection of a low-birefringence nematic liquid crystal. *Liq Cryst*. **2016**;43:427–435.
- [210] Takahashi K, Kimura Y. Dynamics of colloidal particles in electrohydrodynamic convection of nematic liquid crystal. *Phys Rev E*. **2014**;90:012502.
- [211] Hidaka Y, Hashiguchi M, Oikawa N, et al. Lagrangian chaos and particle diffusion in electroconvection of planar nematic liquid crystals. *Phys Rev E*. **2015**;92:032909.
- [212] Suzuki M, Sueto H, Hosokawa Y, et al. Duality of diffusion dynamics in particle motion in soft-mode turbulence. *Phys Rev E*. **2013**;88:042147.